



Global precipitation measurement: Methods, datasets and applications

Francisco J. Tapiador ^{a,*}, F.J. Turk ^b, Walt Petersen ^c, Arthur Y. Hou ^d, Eduardo García-Ortega ^e, Luiz A.T. Machado ^f, Carlos F. Angelis ^g, Paola Salio ^h, Chris Kidd ^{i,d}, George J. Huffman ^{j,d}, Manuel de Castro ^a

^a Department of Environmental Sciences, UCLM, Toledo, Spain

^b Jet Propulsion Laboratory, California Institute of Technology, Pasadena, CA, USA

^c NASA Goddard Space Flight Center (GSFC)/Wallops Flight Facility, Wallops Island, VA, USA

^d NASA Goddard Space Flight Center (GSFC), Greenbelt, MD, USA

^e Department of Physics, University of León, León, Spain

^f Centro de Previsão de Tempo e Estudos Climáticos, INPE, SP, Brazil

^g Centro de Monitoramento e Alertas de Desastres Naturais, CEMADEN, SP, Brazil

^h Departamento de Ciencias de la Atmósfera y los Océanos, FCEN, University of Buenos Aires, Buenos Aires, Argentina

ⁱ Earth System Science Interdisciplinary Center, University of Maryland, College Park, MD, USA

^j Science Systems and Applications, Inc., Lanham, MD, USA

ARTICLE INFO

Article history:

Received 17 October 2011

Received in revised form 31 October 2011

Accepted 31 October 2011

Keywords:

Precipitation Regional Climate Models (RCM)

Global Climate Models (GCM)

Quantitative Precipitation Estimation (QPE)

Global Precipitation Measurement (GPM)

mission

ABSTRACT

This paper explores the many aspects of precipitation measurement that are relevant to providing an accurate global assessment of this important environmental parameter. Methods discussed include ground data, satellite estimates and numerical models. First, the methods for measuring, estimating, and modeling precipitation are discussed. Then, the most relevant datasets gathering precipitation information from those three sources are presented. The third part of the paper illustrates a number of the many applications of those measurements and databases, namely hydropower, data assimilation and validation of Regional Climate Models (RCM). The aim of the paper is to organize the many links and feedbacks between precipitation measurement, estimation and modeling, indicating the uncertainties and limitations of each technique in order to identify areas requiring further attention, and to show the limits within which datasets can be used. Special emphasis is put on the central role of the upcoming Global Precipitation Measurement (GPM) mission in precipitation science.

© 2011 Elsevier B.V. All rights reserved.

Contents

1. Introduction	71
2. Ground observations of precipitation	72
2.1. Rain gauges	72
2.1.1. Rain gauges in satellite ground validation (GV)	73
2.2. Disdrometers	74
2.3. Ground radars	76

* Corresponding author.

E-mail addresses: francisco.tapiador@uclm.es (F.J. Tapiador), joseph.turk@jpl.nasa.gov (F.J. Turk), walt.petersen@nasa.gov (W. Petersen), arthur.y.hou@nasa.gov (A.Y. Hou), eduardo.garcia@unileon.es (E. García-Ortega), luiz.machado@cptec.inpe.br (L.A.T. Machado), angelis@cptec.inpe.br (C.F. Angelis), salio@cima.fcen.uba.ar (P. Salio), chris.kidd@nasa.gov (C. Kidd), george.j.huffman@nasa.gov (G.J. Huffman), manuel.castro@uclm.es (M. de Castro).

3.	Satellite estimates	77
3.1.	Infrared-based methods	77
3.2.	Microwave techniques	77
3.2.1.	Passive microwave (PMW) methods	78
3.2.2.	Active microwave sensors: spaceborne radars	79
3.2.3.	Merged techniques	79
4.	Modeling	80
4.1.	General Circulation Models (GCMs)	81
4.2.	Reanalyses	81
4.3.	Regional Climate Models (RCMs)	81
4.4.	Ensemble methods	82
5.	Datasets of global precipitation	82
5.1.	Observational databases	82
5.1.1.	CRU	87
5.1.2.	GPCP	87
5.1.3.	GPCP	87
5.1.4.	CPC PREC/L DATA	88
5.1.5.	CMAP	88
5.1.6.	TRMM products	88
5.2.	Model datasets	89
5.3.	Global Climate Models (GCMs)	90
5.3.1.	Reanalyses	90
5.4.	Databases of Regional Climate Models	91
6.	Applications of global precipitation measurements	92
6.1.	Hydropower	92
6.2.	Data assimilation into NWP models	93
6.3.	RCM validation	94
7.	Outlook	94
	Acknowledgements	94
	References	94

1. Introduction

Today, precipitation science is at the crossroads of different scientific disciplines including among others hydrology, numerical modeling, climate change, remote sensing, forecasting and more recent innovations such as renewable energy research. Research directions range from improving the description of rain microphysics for climate change studies to areal interpolation of surface rain for agricultural applications, to name but two quite different approaches.

Rainfall and solid precipitation at the basin scale are the primary input to hydrological models predicting stream flow when used to manage hydropower operations. Early warning systems for landslides also require a good knowledge of recent precipitation, while in agriculture, irrigation scheduling is contingent upon recent and expected rainfall in the near future, especially in semiarid environments. In the realm of weather, precipitation estimates are used for nowcasting and for assimilation into global and regional models, aiming to improve the forecasts of not only precipitation but other variables such as temperature, evaporation and wind speed.

In the field of climate change assessment, apart from the intrinsic importance of detecting changes in water availability in the future, precipitation is routinely used to gauge the skill of model simulations, a task which is realized by comparing the climatology of present-climate simulations with that of observational datasets. Also, precipitation estimates over land and the oceans are instrumental to closing the global water cycle.

Both measuring and forecasting precipitation are important for these and other applications. Prediction might be seen as clearly preferable as it allows for the preparation of future events. However, improving the skill of the forecasts is closely intertwined with the ability to measure precipitation. The better the precipitation measurement, the better the likelihood of improved forecasts of precipitation and other meteorological parameters. Here, an area of fertile exchange is model parameterization, as the advances in the physics of precipitation required to improve numerical models heavily rely on testing new hypotheses by actual measurements of precipitation. This is particularly the case of, for instance, theoretical parameterizations of rain microphysics used in models, which should be consistent with ground or in-situ observations.

Given the breadth of the applications and their importance for human activities, the interest and effort devoted to accurate precipitation monitoring is not surprising. The growing importance of the field, however, runs in parallel with difficulties in the actual measurement. Precipitation is a very difficult variable to estimate both because of its irregular spatial occurrence, and also due to very diverse physical processes. For example, while cold and warm-based clouds both eventually generate precipitation, the processes leading to the formation of the liquid water are quite different. Such diverse meteorological conditions present a challenge to space-based remote sensing techniques for estimating precipitation.

Scientific advancements in quantitative precipitation estimation and their applications throughout the last decade

have crystallized into the Global Precipitation Measurement (GPM) mission, organized as an international project led by the National Aeronautics and Space Administration (NASA, USA) and the Japanese Space Agency (JAXA, Japan). Given its approaching launch date (February 14, 2014), it seems timely for this paper to organize the many links and feedbacks between precipitation measurement, estimation and modeling, focusing on those methods suitable for generating a picture of global precipitation patterns. The body of this paper is organized in three sections. First, the methods for measuring, estimating, and modeling precipitation are discussed. Then, the most relevant datasets gathering precipitation information from those three sources are presented. The third part of the paper illustrates a few of the many applications of the databases.

Within the paper, the term *measurement* is used depending on context as a general term or to specify the direct physical readings of precipitation, thus being restricted to rain gauges and optical and video disdrometers. *Estimation* refers to inferring precipitation from a measure such as brightness temperature, momentum, or reflectivity, whereas the term *forecasts* is used to the hours to days predictions of numerical weather prediction (NWP) models. *Projections* refers to predictions from seasonal models, and *simulations* to the com-

puter file outputs from either Global Climate Models (GCMs) or Regional Climate Models (RCMs). *Reanalysis* is defined as a retrospective analysis of the atmosphere using data assimilation methods and a numerical model.

2. Ground observations of precipitation

Ground observations of precipitation include those from rain gauges, disdrometers and radars. With a few exceptions which are immaterial on the global scale, these are restricted to land and to a few atolls. Rain gauges are universally considered as the source of reference data for precipitation observations as they provide a direct physical record of the precipitation in a given spot. Disdrometers are a relatively new instrument that estimate not only the total precipitation but also the relative contribution of each drop size category (the drop size distribution, or DSD) to the total, which is an important parameter for microwave-based estimation of precipitation. Both instruments are direct in that they respond to individual drops, but have a fairly small sampling area (tens of square centimeters), which affects the representativeness of the measurements. In contrast, ground radars sample a large volume but provide an estimate of the precipitation based on the backscattered echo, an indirect observation which relates to total rainfall through the DSD.

2.1. Rain gauges

There are several rain gauge types, each one with its own limitations and strengths (cfr. [Strangeways, 2004, 2010](#) for reviews). The tipping bucket type is one of the most common rain gauges. It typically consists of a collecting area that drains into coupled oscillating buckets. Each time one bucket is filled, it discharges the water then producing a signal on an electric circuit. The bucket then is replaced by the other bucket and the process repeats. Each recorded oscillation then corresponds to a small volume of precipitation. Being a mechanical instrument, rain gauges are subject to many potential error sources, which are exacerbated by the fact that only a fraction of such gauges are carefully maintained. They are known to underestimate heavy precipitation, not only because the collection area is relatively small but also because water can accumulate into the collector faster than the buckets are capable of draining it, resulting in a saturation effect at high rainfall rates (above 300 mm h^{-1}) albeit this effect is rare. They are also problematic for light rainfall that may evaporate in the collector or in the bucket, and prone to problems due to leaves jamming the collector, birds or insects, rust or dust in the mechanism, or clock drift, which may affect the timing of the measurements relative to other instruments. Also, for light precipitation, the tip-size and the logger sampling rate are critical to provide proper representation. Rain gauge response to snow or to hail is problematic, as those have to melt to trigger the signal.

Less common are gauges based upon measuring precipitation by weighing the water accumulated at different sampling rates. The saturation effect is then not relevant, but they are modern instruments, more expensive and less common. Other types, such as siphon-based rain gauges exist, but virtually all the reference databases suitable for

72 ANNUAL REGISTER, 1770.

Of the different Quantities of Rain, which appear to fall, at different Heights, over the same Spot of Ground. By William Heberden, M. D. F. R. S.

[Read December 7, 1769.]

A Comparison having been made between the quantity of rain, which fell in two places in London, about a mile distant from one

same house, and there was found the same difference between these two, though placed so near one another, which there had been between them, when placed at similar heights in different parts of the town. After this fact was sufficiently ascertained, it was thought proper to try, whether the difference would be greater at a much greater height; and a rain-gauge was therefore placed upon the

From July the 7th, 1766, to July the 7th, 1767, there fell into a rain-gauge fixed

	Below the top of a house.	Upon the top of a house.	Upon Westminster Abbey.
	inch.	inch.	inch.
1766 from the 7th of July to the end	3,591	3,210	2,311
August	0,558	0,479	} 0,508
September	0,421	0,344	
October	2,364	2,061	1,416
November	1,079	0,842	0,632
December	1,612	1,258	0,994
1767	2,071	1,455	1,035
January	2,864	2,494	1,335
February	1,807	1,303	0,587
March	1,437	1,213	0,994
April	2,432	1,745	1,142
May	1,977	1,426	} 1,145
June	0,395	0,309	
from the 1st of July to the 7th	22,608	18,139	12,099

Fig. 1. (Top) The first scientific communication reporting differences in measured precipitation with height (Heberden 1770). In a series of experiments, Heberden compared the estimates of identical rain gauges at several heights. He first placed two at the same level to ensure consistency and then moved one at different heights. In his final crucial experiment in London, which he carried out for a year he used three rain gauges. One was placed at ground level, another one at the roof of a house above nearby chimneys, and the third at the top of Westminster Abbey nave. (Bottom) The results of Heberden's experiments: a consistent pattern of decreasing measured precipitation with height across both individual episodes, monthly accumulations and annual totals. Differences up to 87.4% were found in just 32 m.

meteorological and climatic research are made up from tipping bucket rain gauges or to direct-reading accumulation gauges.

Apart from errors due to instrumental problems, there are other intrinsic error sources affecting rain gauges. Wind flow effects are one of the major contributors to the error as it modifies the effective cross-section measurement area and consequently introduce a bias in the readings. Turbulence induced by the gauge also influences the measurements and can make the readings unrepresentative of actual rainfall. The wind flow effect is a particular challenge for light rain and snow because the hydrometeors more closely follow the air flow. Also, as wind speed rapidly increases with height into the boundary layer, two rain gauges at different heights will measure different amounts of precipitation, thus requiring careful adjustments to create meaningful rain maps. This effect was already demonstrated in 1769 by William Heberden (Fig. 1). It is now accepted that three dimensional interpolation is required to account for the topographic bias when gridded datasets are derived from station data, not only because the negative height gradient but also because precipitation may increase with height due to orographic effects (Briggs and Cogley, 1996).

Modern experiments better quantify the effect of wind on rain gauge measurements. Using numerical simulations and empirical estimates, Nespor et al. (2000) found that the larger the blockage of the airflow by the gauge body, the larger the error. They also found that error is dependent on drop size and wind speed, with larger errors for rain with larger fractions of smaller drops and for higher wind speeds. In a recent experiment (Ciach, 2003) fifteen rain gauges placed within an 8 m × 8 m square recorded substantial differences between identical instruments, even with such close proximity. To further complicate the issue the errors were found to be highly dependent on rainfall intensity and timescale, meaning that no clear functional relationship with distance can be proposed to adjust for biases.

As reported in New et al. (2000) effects such as undercatch varies with rain gauge type while historical instrument changes result in inhomogeneities in the records. The correction of precipitation data series requires local meteorological and station meta-information, which are often not readily available. The error sources are reasonably well understood and include, for example, basic mechanical and electrical failure, undercatch in heavy rain (i.e., rates exceeding 50 mm h⁻¹ depending on the gauge) and/or strong winds, reduced sensitivity to low rainfall rates, susceptibility to partial or even total blockage of the collection area by biological debris, dynamic changes in calibration and varying degrees of sensitivity to rain rate that often require integration times of 5 min to 15 min or more (Habib et al., 2001; Sieck et al., 2007; Krajewski, 2007).

Another issue regarding the use of rain gauges to generate global databases is the natural variability of precipitation. Precipitation physics develops below the centimeter scale and the statistics cascade up as we aggregate in space. Differences in precipitation at the kilometer scale are noticeable and increase in mountainous areas due to orographic influences. The sparse distribution of the gauges makes interpolation necessary in order to provide estimates over large areas. Interpolated rainfall, however, is seldom representative of

the actual rain field, and the utility of rain gauges to represent areal rainfall has been repeatedly contested. Methods to interpolate point to areal estimates are based on some quantitative estimate of the spatial variability of the fields. An often used quantity, such as the semi-variance, is empirically derived, modeled, or inferred from the climatology, and then applied to the point measurements.

In spite of all these issues, rain gauges still represent the vast majority of the instrumentation available for building reference precipitation datasets. Since they are relatively cheap and easy to install and calibrate, they have been a fundamental instrument for decades, and thus the only available information from which to derive long records of reference precipitation. Future progress on this topic might depend on the combination of very dense observational networks with advances in stochastic modeling aimed at finding a robust method to select the most likely spatial model among a large number of data-consistent structures (Tapiador et al., 2011). Better knowledge of mountain precipitation will also certainly be required to improve interpolations, given the large variability of precipitation with height and the complex orographic effected by the wind flow.

2.1.1. Rain gauges in satellite ground validation (GV)

The use of precipitation gauges as a de facto reference for rainfall measurement and hence satellite ground validation (GV) or climate model verification, has evolved in response to the relatively simple, low-cost, wide-use, and direct measurement provided by single gauges. Many of the ambiguities associated with individual gauge errors in the quality control process and even reduction of measurement random error can be mitigated by collocating multiple gauge at a given site (Krajewski et al., 2003; Ciach and Krajewski, 2006; Habib et al., 2001), however this is typically not a standard practice for most operational networks. From an integrated validation and applications perspective even if a network of rain gauges makes perfect measurements, one must be mindful of point-to-area representativeness errors when upscaling gauge derived point estimates for comparison to area-means computed over satellite footprint scales (0[0.25° × 0.25°] grid), or even smaller areas typical of a radar estimate (4 km²), as these errors can be substantial and must be adequately quantified (Morrissey et al., 1995; Anagnostou et al., 1999; Wood et al., 2000; Moore et al., 2000; Habib and Krajewski, 2002; Ciach and Krajewski, 2006; Hong et al., 2006; Villarini et al., 2008).

For rain gauge networks that are well maintained, regularly calibrated (e.g., at least twice per year), constructed with suitable gauge density, and used at appropriate temporal and spatial averaging scales, the application to problems of satellite GV is relatively robust (cf. review by Ebert et al., 2007). However, such networks are relatively recent and typically found in countries with the necessary infrastructure. Nonetheless, even these networks are also subject to significant sources of error, both intrinsic to the instruments themselves (Veurich et al., 2009) and due to the occasionally difficult operator logistics associated with required maintenance and calibration. Moreover, the overwhelming majority of rain gauge networks consist of individual instruments. In practice, quality control of individual gauges that may be

only marginally performing (e.g., partially blocked funnel in a tipping bucket gauge) in such networks is difficult at best.

2.2. Disdrometers

A more physical approach useful for satellite comparisons demands that we ascertain the fundamental properties of the medium we are trying to observe. Specifically, it is of interest to identify the coupling between key physical properties of the precipitation (e.g., DSD, particle shape) and the remotely sensed variables of interest. The need for DSD studies using disdrometers span applications related to validating DSD assumptions and implicit impacts on retrieval sensitivities found in various components of satellite-based precipitation retrieval algorithms (Grecu et al., 2004; Iguchi et al., 2009), and verifying the calibration of DSD retrieval algorithms using polarimetric radar (Bringi et al., 2009).

For this particular problem disdrometers provide a means to quantify DSD and individual hydrometeor physics across a multitude of precipitation types (Tokay and Short, 1996; Yuter et al., 2006; Chang et al., 2009), temporal scales (Tokay and Short, 1996, 2003; 2008), and if deployed in networks, spatial scales (Mirivsky et al., 2004; Tokay and Bashor, 2010; Jaffrain et al., 2011; Tapiador et al., 2010).

In general, disdrometers can be subdivided into two basic types: optical and impact sensors. The most common impact disdrometer type is the Joss–Waldvogel disdrometer (JW) (Joss and Waldvogel, 1967), with a more recent instrument for rainfall rate measurement (and only coarse representation of the DSD) being the Vaisala WXT-510 model. The JW has been traditionally used as a reference in numerous studies of the DSD, and in particular, relationships between the DSD measurement and the equivalent radar reflectivity factor (Z) in efforts to assess/calibrate climatological rainrate relationships (Z – R relations) (Tokay and Short, 1996).

Impact disdrometers rely on piezoelectric measurements of individual drop impacts on a Styrofoam cone with an area of 50 cm^2 and assume a fixed fall speed, typically based on (Gunn and Kinze, 1949). Number concentration and fallspeeds are used to compute products such as rain rate, reflectivity, liquid water content etc. when multiplied by an appropriate moment of the DSD. Noted weaknesses of the JW include sensitivity to acoustic noise and its impact on DSD measurements on the small drop end of the spectrum (e.g., $<0.7\text{ mm}$), inability to resolve the large end of the DSD spectrum (e.g., diameters $>5\text{ mm}$), and recovery *dead time* during heavy rainfall events.

Complementing the impact disdrometers such as the JW are oft-used optical disdrometers including the OTT Parsivel (Löffler-Mang and Joss, 2000) and Thies disdrometers (Maraes-Frasson et al., 2011) which operate on very similar principles, and finally the 2-dimensional video disdrometer (2DVD) (Schonhuber et al., 2008). At the most basic level, both the Parsivel and Thies disdrometers rely on measurements of the amplitude and duration of a voltage reduction associated with drop extinction of light in a laser sheet as registered by opposing photodiodes (Knollenberg, 1970). Thies disdrometers measure the diameter and fall velocity of individual hydrometeors over size ranges from 0.2 to 8 mm and 0.2 to 10 m s^{-1} over 20 diameter and 22 velocity evenly spaced bins respectively. Parsivel disdrometers

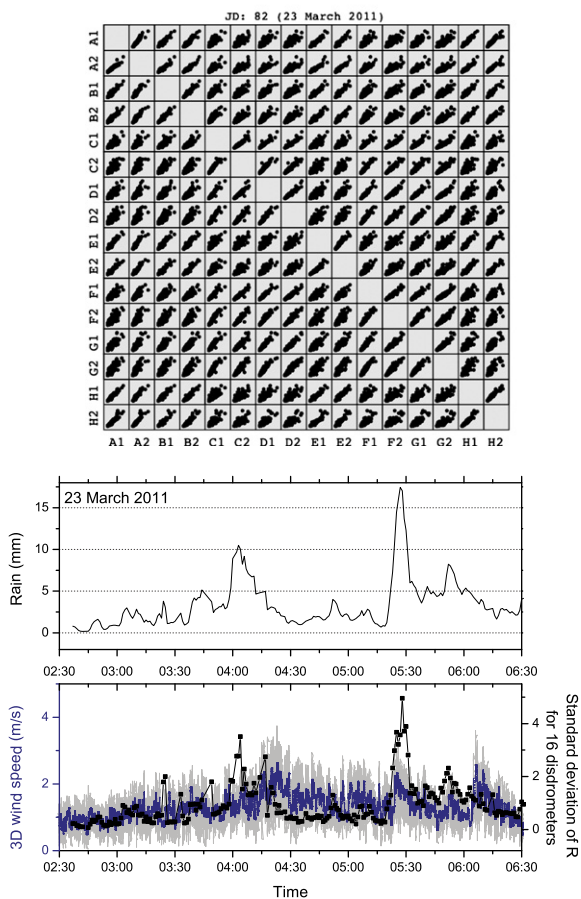


Fig. 2. Experimental setup in Toledo, Spain, to analyze the stability of Parsivel DSD estimates (top). Cross-correlation of the individual estimates from the 16 disdrometers in terms of rain rate for an episode (middle), and (bottom) relationship of the observed variability in rain rate estimate (squared line) of the episode with the turbulence as measured by the co-located 10 Hz sonic anemometer (grey line: original 10 Hz sampling; blue line: moving average). The results provide the first empirical evidence of the short-scale variability of the DSD as being due to turbulence.

measure diameters from 0.2 to 25 mm in a velocity range of $0.2\text{--}20\text{ m s}^{-1}$ over 32 diameter and 32 velocity non uniformly spaced bins.

In contrast, disdrometers such as the 2DVD use high speed orthogonally mounted line scanning cameras oriented

along imaging planes separated by a 6–7 mm vertical distance to infer hydrometeor diameters, fall speeds, shapes and horizontal velocities in the intersection of the camera fields of view. The 2DVD measures drop sizes in user-defined bins over a relatively large $10 \times 10 \text{ cm}^2$, at the finest resolution of $\sim 0.2 \text{ mm}$ and in a diameter range of 0.2 mm to 8 mm. Velocity measurements are accurate to 4% for fall speeds of 10 m s^{-1} or less. Since its inception, the 2DVD has gone through three basic models, beginning with the classic *tall* model and subsequent movement to a *low-profile* version to deal with adverse wind impacts of the tall model (Nespor et al., 2000). More recently Joanneum Inc. produced a third-generation *compact* model designed to be more robust in terms of unattended operation during field deployments. The compact model is currently being used in NASA GPM Ground Validation field campaigns (Petersen et al., 2010) and was rigorously tested and compared relative to collocated second-generation 2DVD datasets in Huntsville, Alabama. Tests indicate nearly identical performance between the second- and third-generation 2DVD (Thurai et al., 2011).

Collectively the DSD requirements provided by the aforementioned disdrometer types are required to test and validate the assumptions of satellite retrieval algorithms which are then combined into global databases. Indeed, these requirements go beyond the provision of providing a single point measurement, sampling at a single point over long timer intervals, or even extension to a single narrow column of the atmosphere. Rather, the need extends to quantification of the 4-D DSD behavior and intrinsic variability at scales ranging from a single satellite pixel to those of mesoscale domains (Greco et al., 2004). Accordingly, studies and instrument facilities deploying networks of disdrometers such as those described in Tapiador et al. (2010) and Jaffrain et al.

(2011), and those being developed within the NASA GPM GV program (Petersen et al., 2010) are the next step in completing broader radar and satellite GV activities. Here the idea is to not only use the disdrometer information as a means to define the natural variability of the DSD over space and time, but also to characterize that variability as it pertains to quantifying measurement error characteristics of the DSD using platforms such as polarimetric radars (Cao et al., 2008; Thurai et al., 2009); the polarimetric radars being a primary physical validation bridge between the disdrometer point measurement and the DSD or rainfall retrieval over the larger footprint of a satellite, for example. In this regard, intercomparisons between individual disdrometers in a network and between disdrometer types will be critical (Tokay et al., 2001; Krajewski et al., 2006; Jaffrain et al., 2011; Thurai et al., 2011; Maraes-Frasson et al., 2011). For example, when compared to rain gauges, JW, and/or 2DVD disdrometer estimates of rainfall, it appears that the current versions of Parsivel and Thies optical disdrometers tend to overestimate rainfall accumulation at heavy rain rates (Lanzinger et al., 2006; Krajewski et al., 2006; Maraes-Frasson et al., 2011; Thurai et al., 2011). In one comparison of the Parsivel to Thies the Parsivel significantly undercounted small drops relative to the Thies in the small drop end of the spectrum (e.g., $< 0.5 \text{ mm}$; Upton and Brawn, 2008). In contrast, Thurai et al. (2011) note a distinct departure in measurement of the mass-weighted mean diameter and mean diameter spectra of the DSD by the Parsivel instrument with rainfall rates of $\sim 20 \text{ mm h}^{-1}$ or greater. The consistency of the Parsivel disdrometers, however, has been proved: experiments with several (16) co-located Parsivels show the stability and coherence of the instrument, and have provided empirical evidence of small-scale (decimeter) variability of the DSD as being due to turbulence (Fig. 2).

Lastly, precipitation is not only limited to liquid forms of precipitation; quantification of frozen precipitation will be especially important in the GPM era. Indeed instrumentation designed to remotely sense snowfall water equivalent (SWE) rates, for example, be it via weighing gauge, radar, or disdrometer have all addressed the challenges to deal with maintenance, calibration, point-to-area representativeness, measurement error, wind, etc., in addition to the irregular shapes, sizes, and bulk density of snowfall. There are ways to retrieve SWE rates over larger areas using combinations of polarimetric radar, disdrometer and weighing gauge data (Brandes et al., 2007; Huang et al., 2010), however doing so is tedious and case specific. As such the next decade of ground-validation science, as it pertains to snowfall measurement, will require large strides in measurement methods and/or technologies to satisfactorily quantify errors not only in the satellite estimates, but errors intrinsic to the instrumentation used and ground validation methodologies/diagnostic approaches used. Solid frozen precipitation types such as hail represents an additional challenge (García-Ortega et al., 2011) due to, for instance, hail being highly localized in space and in time, which makes estimates dependent on the density of the observation network (Sánchez et al., 2009a, 2009b, 2009c; Tuovinen et al., 2009). Hail observations networks for GV using hail-impact meters (Fig. 3) are expensive to maintain and require intensive fieldwork and lab post-processing (García-Ortega et al., 2005, 2006).

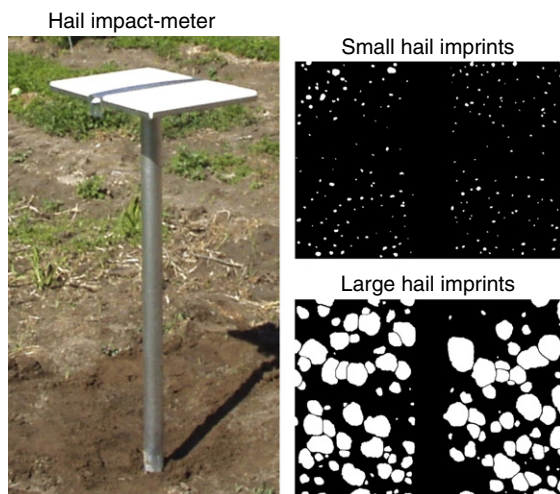


Fig. 3. Hail impact meter (left) consisting in two of pads of foam where hail stones impact and leave an imprint proportional to its size. The figures on the right show two examples of records for small (top-right) and large (bottom-right) hail episodes. The pads are replaced after every hailstorm, and the imprints analyzed using image-processing algorithms in order to derive the hail size distribution.

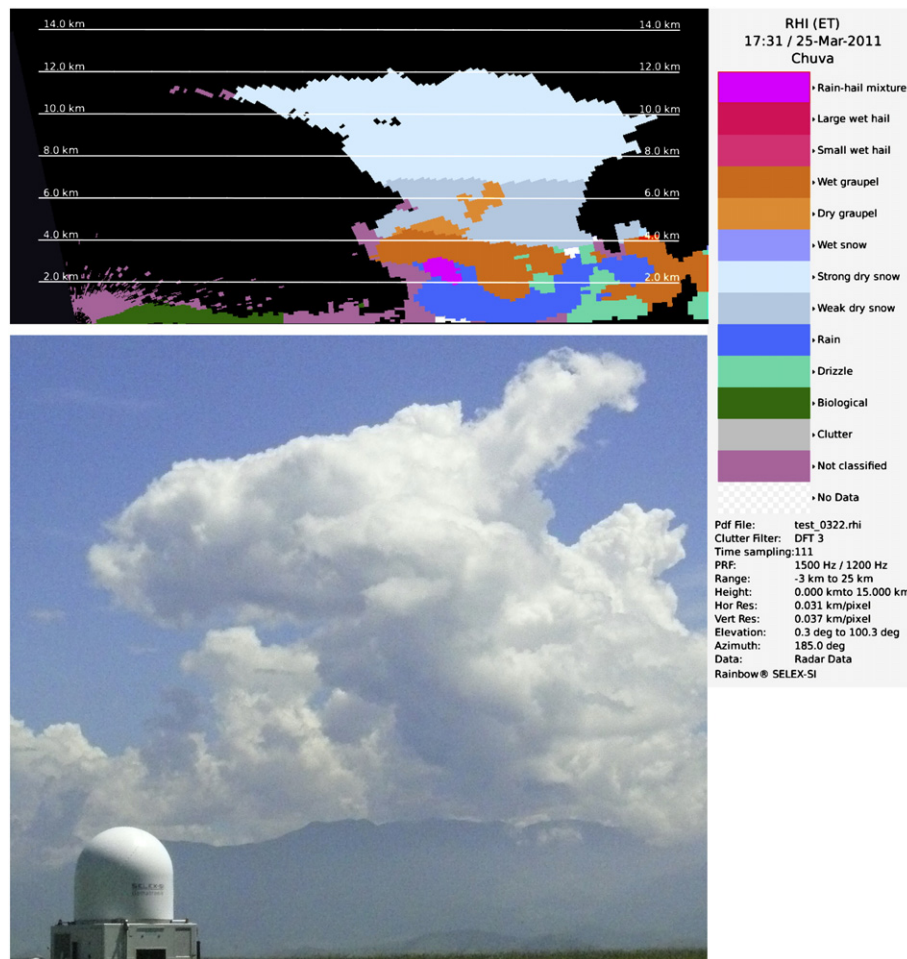


Fig. 4. An example of a cloud classification using an X-band dual polarization radar.
Image credits: INPE, Brazil.

2.3. Ground radars

Deployment of and care for rain gauges deployed in sufficient density to accurately measure rainfall accumulations at scales ranging from sub-hourly to even daily can be a logistically challenging exercise at best. Consequently, ever more sophisticated schemes using radar estimates of precipitation have developed to fill the sampling void. The notion that returned echo power from radar could be used to map rainfall originates from the mid-1940s.

The associated evolution of radar Z–R based approaches to making rainfall estimates on scales of $2\text{ km} \times 2\text{ km}$ has matured such that, when carefully constructed and applied, radar-based estimates can be routinely used to validate satellite estimates of rainfall (Amitai et al., 2011). More recent operational products now include the development of relatively high quality combined rain gauge and radar products. Such combined radar-gauge approaches have been used extensively in the validation process of satellite-based precipitation products created from the Tropical Rainfall Measurement Mission (TRMM) (Wolff et al., 2005).

Direct validation products are often created by time-integrating a measurement of interest (e.g., rainfall measured

by a gauge), often followed by some application of a spatial weighting scheme, including optimal combinations of platform estimates, to create a ground-validation dataset appropriate for statistical comparison to the footprint and time scale of the satellite product in question (cf., Levizzani et al., 2007; Michaelides et al., 2009 for reviews). These GV products are often anchored by the use of precipitation gauge networks of varying spatial density, type and quality (tipping bucket, siphon, weighting etc.).

With the advent of widespread and reliable operational national radar networks, typically composed of C-band to S-band wavelengths, many direct validation efforts now use the point observation of rainfall provided by a rain gauge measurement as a tuning metric for Z–R estimates, which are subsequently used to extend area-mean precipitation estimates to a much larger sampling domain, thus providing more robust statistics for the satellite validation effort. The rapid growth in polarization-enabled radars for research and operational use now affords the opportunity to reduce fundamental and limiting errors in Z–R approaches for estimation of rainfall due to the intrinsic ability of, in particular, dual-polarization radar to account for hydrometeor phase (liquid, melting, or frozen, Fig. 4) and changes in drop size

distribution (DSD) variability within individual storm systems and between meteorological regimes (Bringi and Chandrasekar, 2001; Ryzhkov et al., 2005; Chandrasekar et al., 2008). Broader domain applications to physical validation of DSD properties are also possible (Bringi et al., 2003, 2009; Chandrasekar et al., 2008; Thurai et al., 2011). Moreover, the self consistency of polarimetric variables provides an added means to ensure calibration of the radar measurements. Where appropriately applied (i.e., recognizing the realistic constraints of a radar measurement as a function of range and sampling), it is not unreasonable to imagine future combined gauge and polarimetric radar estimates to provide area mean rainfall and DSD products with total errors of order 15% or less at nearly instantaneous timescales, with rainfall accumulation errors of less than 10–20% (comparable to gauge errors) on scales of 1-hour or better over a 2 km × 2 km grid within 100 km of a given polarimetric radar (Petersen et al., 1999; Bringi and Chandrasekar, 2001; Ryzhkov et al., 2005; Moreau et al., 2009). Assessment of the accuracy of polarimetric radar or combined estimates relative to an independent rain gauge reference will still require a fundamental understanding of rainfall variability, instrument estimation errors, and characterization of all error variance contributions as a function of scale and rainfall type. As demonstrated in recent radar studies (Moreau et al., 2009; Bringi et al., 2009), it is possible to determine these errors, and therefore it is likely that future polarimetric radar estimates will provide high quality data sets, including estimation uncertainties, for validation of satellite-based estimates of rainfall.

3. Satellite estimates

Sensors onboard low-Earth orbiting satellites are the only instruments capable of retrieving global and relatively homogeneous estimates of precipitation. Early statistical or qualitative forms of precipitation measurement have steadily progressed towards more direct methods and more physically based algorithms. The methods used to derive precipitation from the radiances measured by the satellites have evolved from visible (VIS) and infrared (IR) based methods to active and passive microwave (MW) techniques and merged IR and MW approaches.

3.1. Infrared-based methods

Current IR-based methods to derive precipitation from satellites have the advantage of providing high temporal sampling (i.e. 15 min refresh for the Meteosat Second Generation geostationary satellites operated by EUMETSAT), fine spatial resolution (down to 3 km), and for geostationary platforms, wide coverage. The rationale of the estimation method is that cold cloud tops indicate large vertical development of the cloud and therefore more rain. However, the relationship between the cold cloud tops and surface rainfall is indirect and often the location of the coldest clouds is not collocated with the heaviest surface rainfall. The problem is further complicated by multi-layer cloud systems that may block the view of the cloud layer that is actually precipitating.

High, cold, non-precipitating cirrus clouds are also a persistent problem and must to be screened, a strategy only

straightforward if visible and/or Near Infrared (NIR) information is used. These channels provide some microphysical information for satellite algorithms such as an estimate of the effective drop radius at cloud top, but visible channels cannot be used at night and close to the day/night terminator.

The solution of combining several algorithms using different wavelengths for different parts of the day may help meteorological operations, but introduces a bias that make those products less suitable for climate-quality applications. Another known problem for IR methods is that the statistical relationship between cloud top temperature and ground rainfall is highly dependent on season and location. Early operational methods such as the Global Precipitation Index (GPI) (Arkin and Meisner, 1987), the Convective/Stratiform (CST) technique (Adler and Negri, 1988), the Autoestimator (Vicente et al., 1998), and the Hydroestimator (Scofield and Kuligowski, 2003) have to cope with this variability and require a specific calibration to perform well. Resorting to empirical data, however, limits an algorithm's applicability in global climate studies.

Alternative approaches for deriving a relationship between precipitation and IR radiances aloft include the use of clusters or feature extractions. Clouds are systems organized in several space–time scales, from a few meters to thousands kilometers and from minutes to days. This fact allows precipitation to be associated to the resulting clusters. As an example, Machado and Rossow (1993) investigated the distribution of cloud clusters for the regions covered by the Geostationary Operational Earth Satellite (GOES), the Geostationary Meteorological Satellite (GMS) and Meteosat. They found that the number of cloud clusters can be expressed as a function of the cloud radius and that the relationship can be approximated by a power law with an exponent of -2 . This size distribution means a nearly equal area is covered by each effective radius class up to a break radius where size distributions slope becomes much steeper. This break can be interpreted as the end scale of the cloud cover organization over the Earth. This size distribution includes different kinds of synoptic – mesoscale cloud organization as well the cloud cluster evolution during the life cycle.

Another useful observation to inform algorithms is the nearly linear relationship between space and time scale of cloud clusters. In the tropics, the cloud cluster radius has been found to be as linearly related to the average lifetime. Thus for instance systems with a 6-h lifetime have an average radius of 150 km, whereas systems with a 27-h lifetime have a mean radius of 270 km (Machado et al., 1998). Within its lifetime, clouds evolve having different proportion of hydrometeors from the initiation to the decay phase. Empirical evidence exists: Machado and Martins (2008) used S-Band radar data collected during the RACCI/LBA experiment in the Amazon to describe the reflectivity profile of the long lived rain cells as a function of the lifecycle.

3.2. Microwave techniques

A more direct approach to estimate precipitation from satellites involves measurements at microwave and millimeter-wave frequencies, roughly between Ku (10 GHz) and W (95 GHz) bands, although frequencies above and below this are used in some instances. Within this spectral

range, cloud and precipitation-sized particles emit, absorb and scatter radiation. Microwave satellite sensors can either measure the net thermal emission emanating from the top of the atmosphere (passive microwave, or PMW techniques), or measure the power backscattered from a transmitted series of pulses (active microwave techniques).

3.2.1. Passive microwave (PMW) methods

PMW techniques exploit the fact that microwave radiation emitted from the surface interacts with atmospheric constituents such as water vapor and distributed clouds and precipitation particles. Depending on the frequency of the MW radiation, scattering or emission dominates the signal measured by the sensor. Thus, the measurement is the desired signal from the atmospheric constituents mixed with the radiometric contribution from the Earth's surface. Depending upon the surface emissivity, the relative contribution of the hydrometeor-affected signal to the overall received signal can be small, and surface emission can dominate, especially over land.

Emission-based techniques are used over ocean with frequencies below about 20 GHz. At these wavelengths, the ocean is radiometrically cool and the presence of liquid phase precipitation produces an overall warming in the top-of-atmosphere radiation measured by the radiometer. Emission methods are not used over land because it has high surface emissivity, nor can it be employed for high rainfall rates

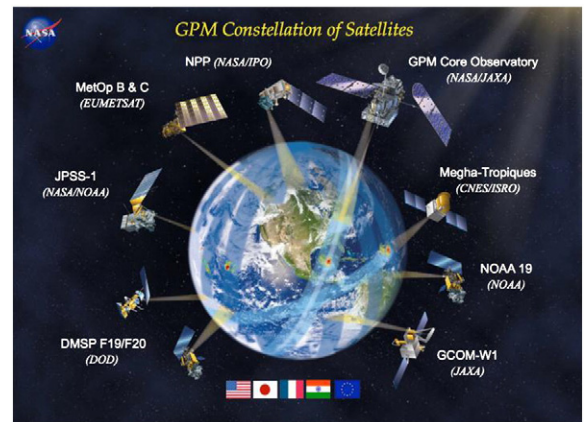


Fig. 6. Illustration of the multiple precipitation measurement satellites which comprise the GPM constellation. Image credits: NASA.

as the relative contribution of hydrometeors to the emission signature saturates exponentially with increasing optical depth.

An indirect scattering-based approach can be used both over land and ocean. Frozen precipitation scatters the upwelling thermal microwave radiation away from the satellite field of view, resulting in a distinct radiometric cooling especially

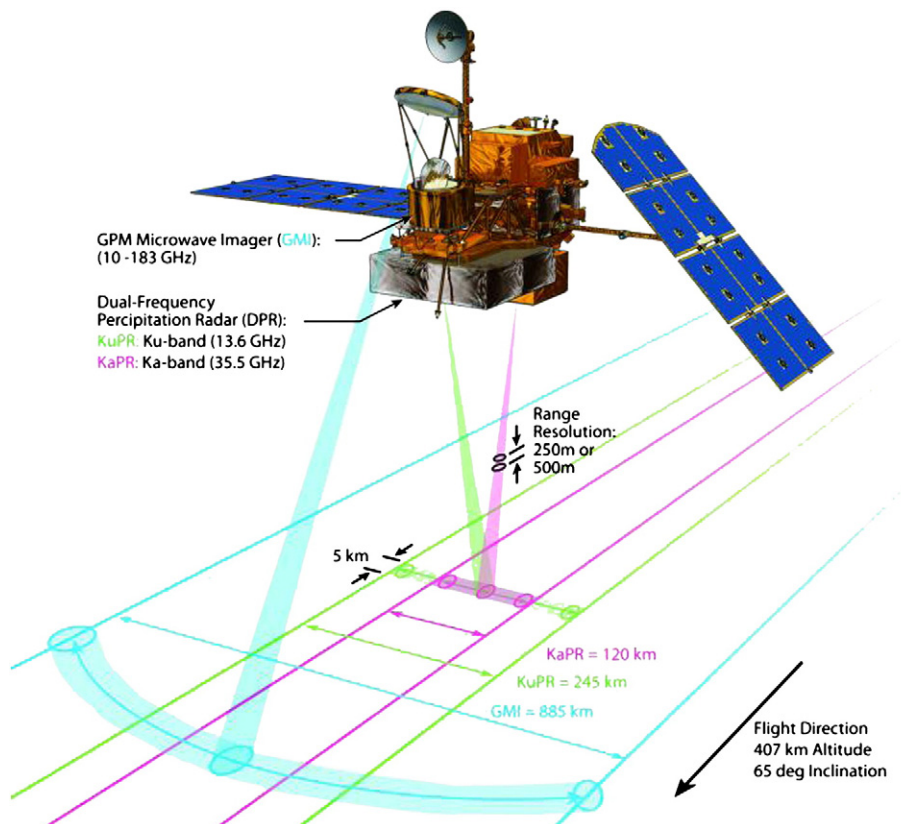


Fig. 5. Diagram of swath coverage by GPM core satellite sensors. Image credits: NASA.

for convective type precipitation. Somewhat similar to IR techniques, the scattering signal at high frequencies (typically near 85 GHz) is dependent on the ice above the freezing layer. Unlike IR techniques however, the thermal emission is more closely related to rainfall processes and hence surface rainfall. Rainfall from cold clouds comes from melted solid phase water, making scattering techniques useful for high latitudes.

While the subject of microwave-based precipitation retrieval techniques is beyond the scope of this article, most modern algorithms are built around simulated databases, which themselves are based on radiative transfer calculations (Elsaesser and Kummerow, 2008) to build a database of simulated observations and their associated geophysical parameters, and then Bayesian or other probabilistic-type methods are used to select the best fits to measured radiances.

A fundamental issue with MW sensors that affects estimation error is that in order to maintain a reasonable antenna size, sensors onboard low orbit satellites have a fairly coarse spatial resolution (anywhere from 5 to 60 km), and the limited fields of view for low Earth orbits reduces their temporal revisit over any given location.

An associated problem to this engineering constraint is the beam-filling effect (Kummerow, 1998), which arises when only a fraction of the large Instantaneous Field of View (IFOV) of the sensor is filled with precipitation, which is common with convective precipitation situations. Unless accounted for, the combined effect of the spatial inhomogeneity of rainfall rates and the nonlinear dependence between MW brightness temperature and rain rate introduces a bias in the retrieval (Wilheit et al., 1991; Chiu et al., 1993).

3.2.2. Active microwave sensors: spaceborne radars

The first spaceborne precipitation radar was the Ku-band TRMM Precipitation Radar (PR) which has operated since 1997; this is extensively reviewed in the literature (Michaelides et al., 2009; Prigent, 2010). The CloudSat satellite, launched in 2006, carries the first W-band cloud radar, capable of quantifying cloud properties and light rainfall rates along the orbit nadir track (i.e. a non-scanning radar). Its orbit in the A-train constellation makes CloudSat a complementary source of information to the fully fledged, precipitation-oriented TRMM satellite and to the AMSR-E radiometer onboard the Aqua satellite.

The many approaches proposed in the last decade to build upon the success of the TRMM era have crystallized into the Global Precipitation Measurement (GPM) mission. It will be launched in February 2014, and is organized as an international project led by the National Aeronautics and Space Administration (NASA, USA) and the Japanese Space Agency (JAXA, Japan). The GPM mission consists of a core satellite (Fig. 5) in non-sun-synchronous orbit (65° inclination on a 407 km-high circular orbit) with a dual-frequency precipitation radar (DPR) and a microwave radiometer (GPM Microwave Imager, GMI). The combination of radar and radiometric methods has already proved useful with TRMM TMI and PR instruments. The DPR will improve the single-frequency radar capabilities of the TRMM era, providing estimates of the shape and size of hydrometeors and the water phase. In addition to the dual frequency (Ku/Ka-band) radar capability, the DPR can also scan in an interlaced mode with

higher sensitivity at Ka-band for detection of light rain and snow.

The remainder of the GPM constellation (Fig. 6) is comprised of a number of satellites with GMI-like radiometers or microwave sounding instruments, including the DMSP F19 and F20 (U.S. DoD; imager), GCOM-W1 (JAXA; imager), JPSS-1 (NASA/NOAA; sounder), Megha-Tropiques (CNES/ISRO; imager and sounder), MetOp B and C (EUMETSAT; sounder), NOAA 19 (NOAA; sounder) and NPP (NASA/NOAA; sounder) satellites. The GPM core satellite sensors will be used as a reference to intercalibrate the partner constellation radiometers, thus providing self-consistent radiometric observations across the constellation.

3.2.3. Merged techniques

The development of single-channel or single-sensor techniques for estimating precipitation has a number of advantages, notably simplicity in algorithm design. However, such techniques are often limited in their frequency of observation, only several times per day for low-Earth orbits. As mentioned above, techniques using visible channels rely essentially on the presence/absence of cloud, while the infrared techniques rely primarily upon the temperature of the cloud tops. Although techniques based upon PMW sensors provide more direct observations of the hydrometeors that form precipitation, these observations are of limited availability. The dichotomy of Vis/IR and PMW observations has been emphasized in a number of algorithm intercomparisons that have been carried out which showed that PMW techniques provide the best instantaneous estimates of precipitation, while Vis/IR techniques provide the best longer-term estimates (Ebert, 2007).

The combination of Vis/IR and PMW observations was therefore seen as an opportunity to combine the good sampling (Vis/IR) with better retrievals (PMW) to provide not only better estimates overall, but estimates with improved temporal and spatial resolution. Initial studies of incorporating PMW estimates into existing Vis/IR schemes included Bristol-NOAA InterActive Scheme (BIAS) (Barrett et al., 1987) where PMW estimates replaced Vis/IR estimates of precipitation and were then interactively advected using cloud development and movement. (Adler et al., 1993) used the PMW estimates to calibrate IR cloud top temperatures allowing regional-scale corrections to be made. Such IR-calibrated techniques were generated at relatively coarse resolutions (about $2.5^\circ \times 2.5^\circ$) at monthly time scales. Increases in computing power and data storage meant that the acquisition, storage and processing of large data sets became more feasible, and opened the possibility of developing higher temporal and spatial resolution products.

Current techniques that combine information from the Vis/IR and PMW fall broadly into two main categories. The first are a development of the initial PMW calibration of the IR observations. Such techniques include the NRL-Blended technique (Turk and Mehta, 2007) and the Passive Microwave-InfraRed (PMIR) technique (Kidd et al., 2003). These techniques use a moving spatial and temporal window to generate a local relationship between the IR observations and the precipitation estimates sourced from PMW observations. The TRMM Multi-Satellite Precipitation Analysis (TMPA; Huffman et al., 2007) provides four products: a

merged-microwave product, a microwave-calibrated IR product, a combined merged-microwave product, and lastly a raingauge-adjusted product. PMW-calibrated IR techniques rely on the ability of the PMW to capture the precipitation characteristics and for the IR to faithfully track the precipitation distribution. In order to improve the retrieval ability of the Vis/IR part of the merged scheme some techniques have utilized artificial neural networks (ANN). As an example, the Precipitation Estimation from Remote-Sensed Information using ANN (PERSIANN; Sorooshian et al., 2000) uses multi-source information from satellite and surface data sets to establish, and update the relationship between the precipitation and Vis/IR observations. A discussion of the use of ANN in rainfall estimation can be found in Tapiador et al. (2004).

The second major category of merged techniques are the advection or Lagrangian time-interpolation schemes. Examples of such schemes include CMORPH (Joyce et al., 2004), GSMaP (Kubota et al., 2007) and REFAME (Behrangi et al., 2010). These techniques are based on the fact that PMW estimates provide the best measure of precipitation, relying upon the IR observations to provide information about the movement of the precipitation system. Thus these techniques are broken down into a number of stages including the generation of the precipitation estimate from the PMW data, and the generation on the motion vectors from the IR observations. Vector techniques currently used in operational products are correlation- or mesh-based techniques (Bellerby, 2006) and the morphing of the estimates between the overpass times of the available PMW observations (Joyce et al., 2004). More physically based approaches based linearizations of fluid dynamic equations (optical flow techniques) have been suggested for this purpose (Tapiador, 2008). These merged scheme currently produce precipitation products at a nominal resolution of 3-hourly, 0.25° , although finer resolution data products are available up to the resolution/sampling of the component data sets.

4. Modeling

Direct observation and estimation of precipitation are important to provide a realistic picture of the several components of the water cycle. However, they cannot be used to predict ahead at the temporal and spatial scales required for most scientific studies and applications. The location and timing of model predicted precipitation, on the other hand, often bears little resemblance with observed patterns except when averaged over fairly coarse scales.

Models predict precipitation after solving many physical processes. Typically, a model works as follows. From a set of 3D initial and boundary conditions of temperature, air moisture, horizontal wind and geopotential in several pressure levels the model solves linearized forms of the non-linear differential equations (called primitive equations) that express the conservation of mass, energy and momentum. Those variables are said to be prognosed (forecasted) at every time step of the model, i.e. stepped forward in time. Other variables such as the state variables are said to be diagnosed, meaning that their values are calculated at once from the instantaneous values, usually using different time steps than the model time step.

Since many physical processes operate below the grid resolution, it is necessary to parameterize many of the diagnosed quantities. For instance, cumulus convection can only be resolved at the kilometer scale. Models using a grid larger than about 5 km need to parameterize the process, meaning that a value has to be provide a sensible estimate of convective precipitation without solving the whole set of equations that describe convection. The same applies to turbulence, which operates at the Kolmogorov scale and also affects precipitation, or to surface processes such as runoff or soil moisture, which cannot be efficiently resolved at kilometer scale.

As a consequence of the many steps involved, precipitation is a good proxy of model performance, since the probability of obtaining a good match between modeled and observed precipitation by chance is small. Thus, the model's dynamical core has to be capable of placing the precipitating system in the right place, thermodynamics should diagnose the correct amount of water in the right phase at each time step, advection has to provide the right amount of water in a precise place to create clouds that eventually precipitate, and the parameterizations of turbulence, cumulus, radiation, and surface processes have to be realistic enough that precipitation is possible at a particular grid point. The microphysics has to be sufficiently detailed in order to distinguish between the phase of the hydrometeors, to provide the appropriate conversion efficiencies, and to decide whether precipitable water is to finally precipitate or not. Otherwise, for instance, cold clouds may be too cold for snow to generate rain or warm clouds may generate too much rain too soon. Important processes such as entrainment, or evaporation below cloud base have also to be taken into account into the parameterizations in order to generate rainfall fields that can be compared with observations.

Unrealistic values of parameters such as the roughness length in the boundary layer module would translate into advanced/delayed arrival times for fronts; oversimplified turbulence schemes may result in dissipation of the kinetic energy needed to allow vertical movements, thus affecting the condensation of water vapor into clouds; and incorrect soil moisture or 3D relative humidity can result in missing light rainfall before it arrives to the ground. Having accurate both long-wave and short-wave radiation models is also instrumental as they simulated the energy balance and thus the energy available to the atmospheric dynamics, rain microphysics and thermodynamics.

This complexity of modeled precipitation, and the patchy character of rain fields make this variable a suitable yardstick to gauge model performance. Compared with temperature, for instance, which is a variable included into the initial conditions, prognosed instead of diagnosed, and exhibiting smooth gradients except in fronts, precipitation is more challenging for a model to simulate correctly.

It is worth remembering here that precipitation is not used to initialize the model, but rather is the result of the physics within the model. While an active area of research is the assimilation of precipitation estimates into models (see section below), the assimilation of precipitation is not carried out by inserting it into the initial conditions, but through adjusting the initial condition fields towards a physical state congruent with the observed precipitation.

4.1. General Circulation Models (GCMs)

Outputs from GCMs running from a single set of initial conditions and driven by periodic boundary conditions can only be compared with observations in terms of climatologies, and not on a day-by-day basis. It is the climate produced by such GCMs, and not the individual weather situations, what it makes sense to compare with other data. In the case of GCMs periodically updated with model reanalyses, the comparison with observational databases is possible, but then the results are not fully independent of the observations as these may have been previously assimilated into the forcing reanalysis (below). This effect explains the excellent scores sometimes reported on those comparisons. On the other hand, the consequences of either once-initialized or nudged-to-reanalyses GCM outputs in impact models deserve further attention. While climatologies, spatial statistics, cycles or other periodic components of the series is justified in both cases, coupled models may generate unpredictable modes of resonance in freely running models, thus further increasing the current large uncertainty of for instance crop models (cfr. Rötter et al., 2011 for a review on current uncertainties in crop models). Uncoupled models do not present such potential problems, as they use the final climatology from the GCM to derive the impacts.

4.2. Reanalyses

Model reanalyses provide spatial and temporal homogeneous data that amalgamates all the available high-quality observations through a physically consistent process. The basic idea is to run a model for a very limited time and iterate until the state is consistent with the observations. Reanalyses offer a method to mitigate several shortcomings of observations, chiefly the sparse distribution, as they embed observations using data assimilation methods into a physical model. The best guess (background forecast) created by the model is a representation of the atmospheric state that is the most consistent with observations, which may have a different weight in the final product. Thus, well-observed processes such as mean sea level pressure depends strongly on observations, whereas precipitation is more a product of the model. Also, depending on data availability in time, reanalyses may be using a varying combination of datasets

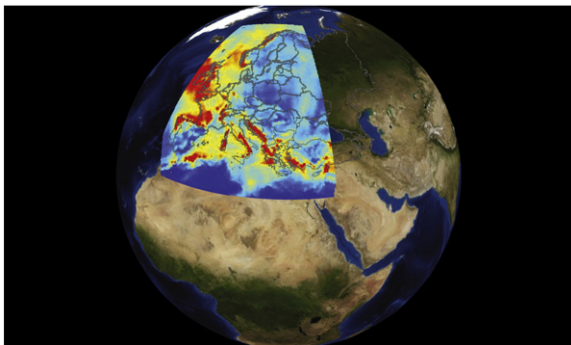


Fig. 7. Geographical domain of the Regional Climate Models involved in the ENSEMBLES project.

(weather stations, aircraft, satellites, etc.) also with a different density of observations for each instrument.

The data quality and the moderate spatial resolution of reanalyses (T159 for ERA40, roughly equivalent to 125 km) make them useful to conduct climate change studies at scales of hundreds of kilometers, and to characterize large scale climatologies of many meteorological variables, since reanalyses estimate derived fields such as evapotranspiration, soil moisture, or shortwave radiation that lack comprehensive observations. Besides, reanalyses are fully tridimensional, thus permitting investigating for instance the genesis of weather systems or the role of columnar water vapor in the radiative forcing.

It is worth remembering that most outputs from reanalyses, or from RCM nested on reanalyses can only be validated using observations if the observations themselves have not been previously assimilated into the reanalysis. Self-reference may happen in spite of precipitation not being nominally assimilated. Simply the fact that clear sky radiances represent the vast majority of the assimilated data implies that information on what constitutes a rainy grid point is being included into the reanalysis. If microwave radiances are assimilated, then the comparison with observational databases is even less independent. While these comparisons are always useful to improve model physics, they do not constitute a verification of model performance.

4.3. Regional Climate Models (RCMs)

For climate studies at scales below hundreds of kilometers where local conditions such as orography and land cover greatly affect meteorological processes, the comparisons of global models with observations are even worse than at coarse spatial resolution. The output from a global model represents the average values for the grid point of the model. If the variable varies smoothly with distance, as is the case of temperature or water vapor content, the average is representative of the values across the grid. However, if the variable has a large spatial variance then quite dissimilar values may coexist within a grid point, making the average an unrepresentative statistic. This problem associated with coarse grids is particularly acute for patchy variables such as precipitation (Pedersen et al., 2010), which are likely to be unevenly distributed in a square often larger than 100×100 km (Larsen et al., 2010). This issue is the modeling analog to the beamfilling problem (Kummerow, 1998) in satellite and radar data.

Regional Climate Models are physically based downscaling tools designed to tackle this problem. The RCM physics and the numerical methods are the same as those in a GCM. The differences are the grid size (from 10 to 75 km) and hence smaller time steps, and a more limited area of operation (e.g. Fig. 7). The geographical domain of the RCM receives initial and boundary conditions from a parent GCM in a procedure known as one-way nesting (Giorgi et al., 1990). However, the improvement of introducing a single RCM does not solve the problem of obtaining better estimates of precipitation, because relevant physical processes at finer resolutions, including cloud and precipitation microphysics, surface processes and turbulence still must be parameterized, as described above. To the extent that these parameterizations contain important simplifications, it is the combination

of several RCMs with different parameterizations which constitutes the most likely climate state.

It has to be remembered that there is a fundamental distinction in nesting the RCM into a GCM or into reanalysis. If nested on GCM boundary conditions (as done in the PRUDENCE project, below), the result can only be treated statistically (i.e., in acimatological sense), and the results reflect the previous limitations of the parent GCM. Nesting on reanalysis and forcing the RCM for a sequence of observed days (as in the ENSEMBLES project, below) is different and generates dynamically-downscaled, observationally consistent climatologies that might even be compared with weather observations. In this case, the model time is not synthetic, 30-day month time as when nested on a GCM, but calendar time. It is also worth mentioning that RCM outputs must be delivered without any bias correction in order to be scientifically usable.

4.4. Ensemble methods

The Perturbed Initial Conditions (PIC) ensemble is a technique consisting in running many numerical simulations (some tens or hundreds) with slightly different initial conditions. The aim is to cope with two unavoidable structural features of atmospheric research, namely sensitivity to initial conditions (SIC), which mainly affects NWP models, and our imperfect modeling of the real world, a problem that is shared by NWP models, GCMs, RCMs and reanalyses.

To address SIC, ensembles are built with a range of perturbed initial conditions. Using techniques such as the bred vectors, the spread of the forecasts is maximized and the whole ensemble clusters around a central value. The spread is indicative of the predictability of the weather, whereas the mean value of the ensemble is deemed to be the least-biased prediction.

Another ensemble strategy, the Perturbed Physics (PP) ensemble, aims to tackle imperfect model physics by running a variety of different models, each one with a different parameterization for key physical processes. Thus for instance, large uncertainties remain in the modeling of the precipitation microphysics used in numerical models so that ensembles of model simulations are generated, each produced by different model physics, and then the results are combined. It is assumed that the shortcomings of the parameterizations are compensated in that way, and that the resulting average outperforms individual models.

The ensemble strategy multiplies computing power requirements, as ensembles of tens or hundreds of members are common. An experiment useful for climate research may involve running a model over a continent such as Europe at 25 kilometer grid space to calculate several decades worth of data. Some weeks of wall clock time are required to complete a 30 year simulation in a 2011 High Performance Computer (HPC). To generate a full PP ensemble, this procedure has to be repeated as many times as ensemble members are desired.

In order to meet growing computing demands, grid computing infrastructure has recently appeared as a powerful tool for precipitation science. The grid strategy consists of distributing the calculations over a large number of regular, not necessarily homogeneous machines connected through a network. HPC systems can act as nodes, thus in a sense

HPC computing is a subset of Grid computing. The grid approach represents an advance loading the computational burden on a highly coupled machine, as a HPC does, and multiplies the computing power and thus enable running more complex models. Even so, it is worth noting that a full multi-ensemble, i.e., running PP ensembles with each member being at its turn a PIC ensemble is not currently feasible due to the computer power required.

5. Datasets of global precipitation

The preceding sections describe satellites and models to provide precipitation data that are accumulated at several temporal and spatial scales to create databases. Such reference datasets are critical to assess the actual uncertainties in climate projections, which are primary tools for global warming studies, by comparing projections with observations and estimates. They are also valuable in their own right to analyze the many aspects of the hydrological cycle, and provide information for economic activities such as agriculture and obviously water resources management.

A number of the precipitation datasets discussed below are publicly available across the Web, although formats and completeness of record vary widely. As a community service, the International Precipitation Working Group (IPWG) of the Coordinating Group for Meteorological Satellites maintains lists of such data sets at <http://www.isac.cnr.it/~ipwg/data/datasets.html>. Also, the Program to Evaluate High Resolution Precipitation Products (PEHRPP) project maintains a web at <http://cics.umd.edu/~msapiano/PEHRPP/index.html> where several datasets are compared. Tables 1–4 group several datasets according to the dominant input data types: they respectively list precipitation gauge analyses (Table 1), single sensor types (Table 2), combinations of satellite data (Table 3) and combinations of satellites and precipitation gauge data (Table 4). Some of the databases are discussed below.

It is worth noting that apart from these global databases there are also regional databases, such as for instance the European Climate Assessment (ECA) for Europe (Klein Tank et al., 2002), or the database described by Liebmann and Allured(2005) for South America.

5.1. Observational databases

The observational databases are based on historical precipitation records from land stations. It is important to note that the original data in the different databases is sometimes the same, the databases differing in how the station records are filtered, interpolated, and homogenized so the agreement is not surprising. Thus, Chen et al.(2002) showed that CRU and GPCP (below) provide reliable information in accumulated monthly precipitation at a global scale, with a close agreement in the phase and the magnitude of the mean annual cycles. However, discrepancies may appear even with the same data depending on the analysis and application. For instance, Qian et al.(2006) reported large differences in the total annual amounts over different rivers basins around the world. The differences may be due to different gauge coverage especially over tropical Africa and tropical South America where the coverage is sparser.

Table 1

Summary of publicly available, quasi-operational, quasi-global precipitation estimates from precipitation gauge data. Where appropriate, the algorithms applied to the individual input data sets are mentioned.

Precipitation gauge analyses						
Algorithm	Input data	Space/time scales	Areal coverage/start date	Update frequency	Latency	Producer (developer) URL
CPC Unified Gauge-based Anal. of Global Daily Precip.	> 30,000 gauges (optimal interp. with orographic effects)	0.5°/daily	Global/1979–2005	–	–	NOAA/NWS CPC (Chen and Xie) [1]
	> 17,000 gauges realtime (optimal interp. with orographic effects)	0.5°/daily	Global/2006	Daily	1 day	NOAA/NWS CPC (Chen and Xie) [2]
CRU Gauge	~12,000 gauges (anomaly analysis)	0.5°/monthly	Global/1900–1998	–	–	U. East Anglia (New and Viner) [3]
CRU TS 2.0 Gauge	~20,000 gauges (anomaly analysis)	2.5° × 3.75°, 5°/monthly	Global/1901–2000	–	–	U. East Anglia (Mitchell) [4]
Dai Gauge Dataset 2	~4000 gauges (anomalies rel. to 1950–1979)	2.5°/monthly	Global regions with data/1850–1996	–	–	NCAR (Dai) [5]
GHCN + CAMS Gauge GPCC Monitoring	~3800 gauges (SPHEREMAP)	2.5°/monthly	Global/1979	Monthly	1 week	NOAA/NWS CPC (Xie) [6]
	~8000 gauges (climatology-anomaly)	1°, 2.5°/monthly	Global/1986–2006 Version 1; 2007 Version 3	Monthly	2 months	DWD GPCC (Becker) [7]
GPCC Full Analysis Version 5	~64,000 gauges (climatology-anomaly)	0.5°, 1°, 2.5°/monthly	Global/1901–2009	Occasional; possible end of 2011	–	DWD GPCC (Becker) [8]
GPCC VASCLimO Version 1.1	~9000 gauges (climatology-anomaly)	0.5°, 1°, 2.5°/monthly	Global/1950–2000	Occasional	–	DWD GPCC (Beck) [9]

[1] ftp://ftp.cpc.ncep.noaa.gov/precip/CPC_UNI_PRCP/GAUGE_GLB/V1.0/.[2] ftp://ftp.cpc.ncep.noaa.gov/precip/CPC_UNI_PRCP/GAUGE_GLB/RT/.[3] <http://www.cru.uea.ac.uk/cru/data/precip/>.[4] http://www.cru.uea.ac.uk/~timm/grid/CRU_TS_2_0.html.[5] http://data.giss.nasa.gov/precip_dai/.

[6] pingping.xie@noaa.gov; Dr. Pingping Xie.

[7] ftp://ftp-anon.dwd.de/pub/data/gpcc/html/monitoring_download.html.[8] ftp://ftp-anon.dwd.de/pub/data/gpcc/html/fulldata_download.html.[9] ftp://ftp-anon.dwd.de/pub/data/gpcc/vasclimo_50y_precip_clim_v1_1.zip.

Table 2

Summary of publicly available, quasi-operational, quasi-global precipitation estimates from a single satellite sensor type. Where appropriate, the algorithms applied to the individual input data sets are mentioned. The GPROF TMI and PR are available as separate products from the Goddard DISC, in addition to the 3G68 compilation.

Single-source data sets						
Algorithm	Input data	Space/time scales	Areal coverage/start date	Update frequency	Latency	Producer (developer) URL
AMP-4	AMSU-A/-B, AMSU/MHS	Level 2 (swath/pixel)/orbit	Global/2002	Orbit (~100 min)	4 h	MIT and Prince of Songkla Univ. (Surussavadee and Staelin) [1]
AMP-5	AMSU-A/-B, AMSU/MHS	Level 2 (swath/pixel)/orbit	Global/2002	Orbit (~100 min)	4 h	MIT and Prince of Songkla Univ. (Surussavadee and Staelin) [1]
GPI	GEO-IR, LEO-IR in GEO gaps	2.5°/monthly	Global – 40 *N-S/1986–Feb. 2004	–	–	NOAA/NWS CPC (Xie) [2]
		GEO-, LEO-IR	2.5°/pentad *N-S/1986–Nov. 2004	–	–	NOAA/NWS CPC (Xie) [3]
GPI	GEO-, LEO-IR	1°/daily	Global – 40 *N-S/Oct. 1996	Monthly	1 week	NOAA/NWS CPC (Xie) [4]
			Global – 70 *N-S/June 2002	Daily	1 day	NSIDC (Kummerow) [5]
GPROF2004	AMSR-E	0.5°/orbits	Global – 70 *N-S/July 1987–Nov. 2009	Daily; monthly	1 day; 1 month	Colo. State Univ. (Kummerow) [6]
GPROF2010	AMSR-E	0.25°/daily (asc. and desc.); 0.25°/monthly	Global – 70 *N-S/June 2002	–	–	Colo. State Univ. (Kummerow) [6]
GPROF2010	SSM/I	0.25°/daily (asc. and desc.); 0.25°/monthly	Global – 70 *N-S/July 1987–Nov. 2009	–	–	Colo. State Univ. (Kummerow) [7]
GPROF2010	SSMIS	0.25°/daily (asc. and desc.); 0.25°/monthly	Global – 70 *N-S/Oct. 2003	Daily; monthly	1 day; 1 month	Colo. State Univ. (Kummerow) [6]
GPROF2010	TMI	0.25°/daily (asc. and desc.); 0.25°/monthly	Global – 40 *N-S/Dec. 1997	Daily; monthly	1 day; 1 month	Colo. State Univ. (Kummerow) [6]
GPROF2010 (3G68)	TMI	0.5°/hourly; 0.1°/hourly land	Global – 40 *N-S/Dec. 1997	Daily	4 days	NASA/GSFC PPS (Kummerow) [8]
HOAPS-3	SSM/I	Swath; 1°/12-hour; 0.5°/pentad, monthly	Global ocean – 80 *N-S/July 1987–2007	Update through 2008 due 2011 by CM-SAF	Not routinely schedule d	HOAPS/Univ. of Hamburg, MPI (Klepp, Andersson) [9]
Hydro-Estimator	GEO-IR	4 km/hourly	Global – 60 *N-S/March 2007	Hourly	3 h	NOAA/NESDIS/STAR (Kuligowski) [10]
METH	SSM/I, SSMIS	2.5°/monthly	Global ocean – 60 *N-S/July 1987–2010	Monthly	1 month	George Mason Univ. (Chiu) [11]
METH (3A11)	TMI	5°/monthly	Global ocean – 40 *N-S/Jan. 1998	Monthly	1 week	NASA/GSFC PPS (Chiu) [8]
MiRS	AMSU/MHS, SSMIS	Swath	Global/Aug. 2007	Orbits; Daily	4 h	NOAA OSDPD (Boukabara) [12]
NESDIS/FNMOCS Scattering index	SSM/I	1.0°/monthly 2.5°/pentad, monthly	Global/July 1987–Nov. 2009	Daily	1–2 h	NESDIS/STAR (Ferraro) [13]
NESDIS High Frequency	AMSU/MHS	0.25°/daily 1.0°/pentad, monthly	Global/2000	Monthly	1 week	NESDIS/STAR (Weng and Ferraro) [14]
OPI	AVHRR	2.5°/daily	Global/1979	Daily	1 day	NOAA/NWS CPC (Xie) [15]
RSS	TMI, AMSRE, SSM/I, SSMIS, QSCAT	0.25°/1-, 3-, 7-day; monthly	Global Ocean – July 1987	1-, 3-, 7-day; monthly	6–12 h; each day, week, month	RSS (Wentz and Hilburn) [16]
TRMM PR Precip (3 G68)	PR	0.5°/hourly	Global – 37°N–S/Dec. 1997	Daily	4 days	NASA/GSFC PPS (Iguchi) [8]

[1] <http://www.aned.psu.ac.th>; <http://web.mit.edu/surusc/www/AP/>.

[2] <ftp://ftp.cpc.ncep.noaa.gov/precip/gpi/monthly/>.

[3] <ftp://ftp.cpc.ncep.noaa.gov/precip/gpi/pentad/>.

[4] <ftp://ftp.cpc.ncep.noaa.gov/precip/gpi/daily/>.

[5] http://nsidc.org/data/ae_rain.html.

[6] <http://rain.atmos.colostate.edu/RAINMAP10/>.

[7] berg@atmos.colostate.edu; Dr. Wesley Berg.

[8] <http://pps.gsfc.nasa.gov>.

[9] <http://www.hoaps.org>.

[10] <http://www.star.nesdis.noaa.gov/smcd/emb/ff/digGlobalData.php>.

[11] <ftp://gpcp-ppspdc.gmu.edu/V6/2.5/>.

[12] <http://mirs.nesdis.noaa.gov>; <http://www.osdpd.noaa.gov/ml/mirs>.

[13] http://www.ncdc.noaa.gov/oa/rsad/ssmi/gridded/index.php?name=data_access.

[14] <http://www.star.nesdis.noaa.gov/corp/scsb/mspps/main.html>; <http://www.osdpd.noaa.gov/ml/mspps/index.html>.

[15] pingping.xie@noaa.gov; Dr. Pingping Xie.

[16] <http://www.ssmi.com>.

Related to this fact, it is worth noting also that topography induces a large error in the evaluation of precipitation regimes. In areas with a dense network the problem is

somewhat masked because the information is dense enough to cope with the spatial variability of the precipitation. Thus for instance CRU over Europe, United States and Canada

Table 3

Summary of publicly available, quasi-operational, quasi-global precipitation estimates that are produced by combining input data from several satellite sensor types. Where appropriate, the algorithms applied to the individual input data sets are mentioned. The TCI is available as a separate product from the Goddard DISC, in addition to the 3G68 compilation.

Satellite combination data sets						
Algorithm	Input data	Space/time scales	Areal coverage/start date	Update interval	Latency	Producer (developer) [URL]
AIRS	AIRS sounding retrievals	Swath/orbit segments	Global/May 2002	Daily	1 day	NASA/GSFC 610 (Susskind) [1]
CMORPH	TMI, AMSR-E, SSM/I, AMSU, IR vectors	8 km/30-min	50°N–S/1998	Daily	18 h	NOAA/CPC (Xie) [2]
GSMaP NRT	TMI, AMSR-E, SSM/I, SSMIS, AMSU, IR vectors	0.1°/hourly	60°N–S/Oct. 2007	1 h	4 h	JAXA (Kachi and Kubota) [3]
GSMaP MWR	TMI, AMSR-E, AMSR, SSM/I, IR vectors	0.25°/hourly, daily, monthly	60°N–S/1998–2006	–	–	JAXA (Aonashi and Kubota) [4]
GSMaP MVK	TMI, AMSR-E, AMSR, SSM/I, SSMIS, AMSU, IR vectors	0.1°/hourly	60°N–S/2000 (currently 2003–2008 data available)	Monthly	Reprocess now; will become operational	JAXA (Ushio) [3]
GSMaP MVK +	TMI, AMSR-E, AMSR, SSM/I, AMSU, IR vectors	0.1°/hourly	60°N–S/2003–2006	–	–	JAXA (Ushio) [4]
NRL Real Time	SSM/I-cal PMM (IR)	0.25°/hourly	Global – 40°N–S/July 2000	Hourly	3 h	NRL Monterey (Turk) [5]
TCI (3G68)	PR, TMI	0.5°/hourly	Global – 37°N–S/Dec. 1997	Daily	4 days	NASA/GSFC PPS (Haddad) [6]
TOVS	HIRS, MSU	1°/daily	Global/1979–April 2005	Daily	1 month	NASA/GSFC 610 (Susskind) [1]
TRMM Real-Time HQ (3B40RT)	TMI, TMI-SSM/I, TMIAMSR-E, TMI-AMSU	0.25°/3-hourly	Global – 70°N–S/Feb. 2005	3 h	9 h	NASA/GSFC PPS (Adler and Huffman) [7]
TRMM Real-Time VAR (3B41RT)	MW-VAR	0.25°/hourly	Global – 50°N–S/Feb. 2005	1 h	9 h	NASA/GSFC PPS (Adler and Huffman) [8]
TRMM Real-Time HQVAR (3B42RT)	HQ, MW-VAR	0.25°/3-hourly	Global – 50°N–S/Feb. 2005	3 h	9 h	NASA/GSFC PPS (Adler and Huffman) [9]

[1] joel.susskind-1@nasa.gov; Dr. Joel Susskind.

[2] http://www.cpc.ncep.noaa.gov/products/janowiak/cmorph_description.html.

[3] <http://sharaku.eorc.jaxa.jp/GSMaP/>.

[4] http://sharaku.eorc.jaxa.jp/GSMaP_crest/.

[5] song.yang@nrlmry.navy.mil; Dr. Song Yang.

[6] <ftp://pps.gsfc.nasa.gov/pub/trmmdata/3G/3G68/>.

[7] <ftp://trmmopen.nascom.nasa.gov/pub/merged/combinedMicro/>.

[8] <ftp://trmmopen.nascom.nasa.gov/pub/merged/calibratedIR/>.

[9] <ftp://trmmopen.nascom.nasa.gov/pub/merged/mergeIRMicro/>.

Table 4

Summary of publicly available, quasi-operational, quasi-global precipitation estimates that are produced by combining input data from several sensor types, including satellite sensors and precipitation gauges. Where appropriate, the algorithms applied to the individual input data sets are mentioned.

Combination data sets with gauge data						
Algorithm	Input data	Space/time scales	Areal coverage/start date	Update frequency	Latency	Producer (developer) URL
CAMS/OPI	CMAF-OPI, gauge	2.5°/daily	Global/1979	Monthly	6 h	NOAA/NWS CPC (Xie) [1]
CMAF	OPI, SSM/I, SSMIS, GPI, MSU, gauge, model	2.5°/monthly	Global/1979–Oct. 2010	Seasonal	3 months	NOAA/NWS CPC (Xie) [2]
	OPI, SSM/I, GPI, MSU, gauge, model	2.5°/pentad	Global/1979–Sept. 2009	Seasonal	3 months	NOAA/NWS CPC (Xie) [3]
	OPI, SSM/I, GPI, gauge	2.5°/pentad-RT	Global/2000	Pentad	1 day	NOAA/NWS CPC (Xie) [4]
GPCP One-Degree Daily (Version 1.1)	SSM/I-TMPI (IR), GPCP monthly	1°/daily	Global – 50°N–50°S/Oct. 1997–Sept. 2009	Monthly	3 months	NASA/GSFC 613.1 (Huffman) [5]
GPCP pentad (Version 1.1)	OPI, SSM/I, GPI, MSU, gauge, GPCP monthly	2.5°/5-day	Global/1979–2008	Seasonal	3 months	NOAA/NWS CPC (Xie) [6]
GPCP Version 2.1 Satellite-Gauge (SG)	GPCP-OPI, gauge 1/79–6/87, 12/87 SSM/I-AGPI (IR), gauge, TOVS 7/87–4/05 except 12/87, AIRS 5/05–present	2.5°/monthly	Global/1979–2010	Monthly	2 months	NASA/GSFC 613.1 (Adler and Huffman) [7]
TRMM Plus Other Data (3B43 Version 6)	TCI-TMI, TCI-SSM/I, TCIAMS-R-E, TCI-AMSU, MW-VAR (IR), gauge	0.25°/monthly	Global – 50°N–S/Jan 1998	Monthly	1 week	NASA/GSFC PPS (Adler and Huffman) [8]
TRMM Plus Other Satellites (3B42 Version 6)	TCI-TMI, TCI-SSM/I, TCIAMS-R-E, TCI-AMSU, MW-VAR (IR), V.6 3B43	0.25°/3-hourly	Global – 50°N–S/Jan 1998	Monthly	1 week	NASA/GSFC PPS (Adler and Huffman) [8]
RFE	GPI, NOAA SSM/I, gauge	10 km/daily	Africa/Oct. 2000	Daily	6 h	NOAA/NWS CPC (Xie) [9]
		10 km/daily	South Asia/April 2001	Daily	6 h	NOAA/NWS CPC (Xie) [10]

[1] ftp://ftp.cpc.ncep.noaa.gov/precip/data-req/cams_opi_v0208/.

[2] <ftp://ftp.cpc.ncep.noaa.gov/precip/cmap/monthly/>.

[3] <ftp://ftp.cpc.ncep.noaa.gov/precip/cmap/pentad/>.

[4] ftp://ftp.cpc.ncep.noaa.gov/precip/cmap/pentad_rt/.

[5] <ftp://rsd.gsfc.nasa.gov/pub/1dd-v1.1/>.

[6] ftp://ftp.cpc.ncep.noaa.gov/precip/GPCP_PEN/.

[7] <ftp://precip.gsfc.nasa.gov/pub/gpcp-v2.2/psg/>.

[8] <http://mirador.gsfc.nasa.gov/cgi-bin/mirador/presentNavigation.pl?tree=project&project=TRMM&dataGroup=Gridded>.

[9] ftp://ftp.cpc.ncep.noaa.gov/fews/newalgo_est/.

[10] <ftp://ftp.cpc.ncep.noaa.gov/fews/S.Asia/>.

comprises enough stations to generate realistic fields, but in some other regions of the world (e.g. South America, Africa or Asia) the error over high elevation sites is large. Some databases, such as GPCP version 2 (Adler et al., 2003) has tackled this problem and devised a specific algorithm to correct this effect, whereas others rely on the ability of the interpolation techniques to deal with the issue.

5.1.1. CRU

The Climate Research Unit (CRU) at the University of East Anglia has been created gridded climate datasets that includes precipitation (New et al., 1999, 2000). The original information from stations is interpolated over the continents except over Antarctica, considering a 0.5×0.5 degree global grid covering the period 1901 to 2001 (New et al., 2000). Up to 14,500 stations are used for databases, but the number varies (from 4957 in 1901 to 14,579 in 1981). Although the records are different in each case, for this interpolation records with at least 30 years of data are used. The data are interpolated by first calculating the anomaly to the average of the years 1961–1990. The anomaly is calculated as the percentage value of the monthly accumulated rainfall from the average of 1961–1990 and then the anomaly is interpolated using thin-plate splines as a function of latitude and longitude. All station available over the globe are first weighted as a function of the distance of the grid point with an empirical correlation decay distance coefficient between the available stations. The coefficient used in the present dataset is 450 km for precipitation, this was created to prevent extrapolations to unrealistic values and the precipitation anomaly at the grid point is forced to be zero over regions beyond the 450 km range.

It is worth noting when using CRU as a reference database that gridded values are obtained by applying a smooth fitting in 3D space to available surface observations at stations (New et al., 2000). This interpolation technique changes the spatial autocorrelation of data and introduces a known bias to the results. Additional sources of uncertainty in this dataset include those related to rain gauges problems, such as undercatch due to wind effects, undersampling in mountain areas or areas with a few instruments, and postprocessing artifacts from observational data. Known nominal errors of the database are described in New et al. (1999). Error sources arise from differences in gauge type, in the evaluation of the ratio of solid to liquid precipitation, and the effects of wind conditions and turbulence.

As in the rest of the precipitation databases, a clear understanding of the input data is crucial for a proper use of the data in for instance climate change studies. As an example, CRU exhibits large differences between observed and interpolated data over the Amazon area in the beginning of the twentieth century. The reason is that from 1901 to 1921 the data for the whole area comes from a single station. Ignoring this and several other particularities may result in extracting the wrong conclusions on model performance and even on the sign of the climate change signal.

5.1.2. GPCP

The German Weather Service Global Precipitation Climatology Centre (GPCC) has made available a $0.5^\circ \times 0.5^\circ$ global land-only climatology from 1951 to 2000 period, at monthly temporal resolution. Original data come from the historical

databases of the U.N. Food and Agriculture Organization (FAO) (13,500 stations), the Climatic Research Unit (9500 stations), and the Global Historical Climatology Network (GHCN) (22,600 stations). Additional contribution includes the GPCC-Synop, the CPC-Synop, and Climat-network (Beck et al., 2004). Only station time series with a minimum of 90% data availability during 1951–2000 are used for interpolation using ordinary kriging. This method is deemed to ensure that the estimates are optimized for homogeneity in time and for application in climate variability studies.

The dataset contains nominal error estimates computed as jackknife-error estimates. This error is the difference of the interpolated value of the location of the nearest station, taking only neighboring stations into account, and the observation at that station. In other words, it is what would have been estimated if there were no observation at the point.

5.1.3. GPCP

The GPCP produces several products that are intended to approach Climate Data Record standards. The monthly Satellite-Gauge (SG) precipitation analysis (Huffman et al., 1997, 2010; Adler et al., 2003) provides globally complete estimate at $2.5^\circ \times 2.5^\circ$ resolution from 1979 forward. The precipitation estimates from the 6 am/pm low-orbit satellite SSM/I and SSMIS microwave satellites provide calibration (varying by month and location) for geosynchronous-orbit satellite infrared (IR) data in the latitude band 40°N –S. Outside that band the SSM/I and SSMIS microwave estimates are combined with estimates based on TOVS or AIRS to provide globally complete satellite-only precipitation estimates. The multi-satellite field is combined with a rain-gauge analyses (over land), first adjusting the satellite estimates to the gauge bias and then combining the (adjusted) satellite and gauge fields with inverse error-variance weighting. The gauge analysis is the GPCC Full analysis for the period available, and the Monitoring product thereafter.

The GPCP pentad precipitation analysis (Xie et al., 2003) uses the SG to adjust the pentad CPC Merged Analysis of Precipitation (CMAP) pentad analysis such that the overall magnitude of the pentad product matches the monthly product and the sub-monthly variability in the pentad CMAP product is retained. It is available at $2.5^\circ \times 2.5^\circ$ resolution from 1979 forward. The GPCP One-Degree Daily (1DD) precipitation analysis (Huffman et al., 2001, 2010) is available at $1^\circ \times 1^\circ$ resolution from October 1996 forward. It uses a Threshold-Matched Precipitation Index (TMPI) in the latitude band 40°N –S to produce instantaneous precipitation from the geo-IR brightness temperatures (T_b). The TMPI takes GPROF estimates of precipitation fractional coverage with SSM/I and SSMIS data to choose a (regionally varying) T_b threshold that makes geo-IR fractional coverage equal to that of the GPROF-SSM/I and -SSMIS estimates. Then a single “raining” geo-IR pixel rainrate is computed (again, regionally varying) that makes the full month of TMPI sum to the corresponding SG monthly value. Outside of the 40°N –S band, TOVS and AIRS precipitation estimates are adjusted in terms of frequency of precipitation using GPROF frequencies at 40° latitude and in terms of the amount by the monthly analysis. The SG dataset also includes a combined satellite-gauge precipitation error estimate. (Huffman et al., 1997) reported that

the bias error frequently can be neglected compared to random error (both sampling-based and algorithmic).

5.1.4. CPC PREC/L DATA

The US Climate Prediction Center (CPC) produces, the Monthly Analysis of Global Land Precipitation from 1948 to the Present, at a $0.5^\circ \times 0.5^\circ$ spatial resolution [PREC/L; (Chen et al., 2002), CPC data hereafter]. Original data in this case comes from rain gauges from about 17,000 stations.

The interpolation in this database is performed using the Gandin optimal interpolation (OI) technique. The correlation between the analysis values and withdrawn independent station observations is about 0.8 and the bias is almost 0 for interpolation of monthly precipitation using the OI algorithm (Chen et al., 2002).

5.1.5. CMAP

The CMAP provides monthly land and ocean estimates of global precipitation from rain gauges and satellite precipitation estimates. The spatial resolution of the dataset is $2.5^\circ \times 2.5^\circ$ for the 1979-onwards period. The merging technique is described in (Xie and Arkin, 1996). As stated there, the methodology used reduces random errors by linearly combining satellite estimates using the maximum likelihood method, giving an inversely proportional weight to the linear combination coefficients in relation to the square of the random error of the individual sources. Over global land areas the random error is defined for each time period and grid location by comparing the data source with the rain gauge analysis over the surrounding area. Over oceans, the random error is defined by comparing the data sources with the rain gauge observations over the Pacific atolls. Bias is reduced when the data sources are blended in the second step using a variational blending technique.

5.1.6. TRMM products

The precipitation radar (PR) onboard TRMM was the first orbital radar to estimate precipitation, and has been providing good quality estimates for the tropical regions since

1998. Merging of the TMI radiometer and the PR instrument with other MW sources has been used to extend the spatial coverage beyond the original area. Thus, the Multi-satellite Precipitation Analysis (TMPA) algorithm provides 3-hourly $0.25^\circ \times 0.25^\circ$ latitude/longitude gridded precipitation data for the latitude band $50^\circ \text{N} - 50^\circ \text{S}$ over the period 1998–present (Huffman et al., 2007). It is designed to use as many satellite-based precipitation estimates as possible with calibration to a single sensor. The TMPA is computed twice, first in near-realtime (TRMM product 3B42RT) and then as a post-realtime research-grade product (currently TRMM Version 7 product 3B42) to accommodate different user needs. The 3B42 product uses the (Haddad et al., 1997a, 1997b) combined TRMM Microwave Imager – Precipitation Radar estimates (TRMM product 2B31) for calibration, while the real-time product uses a real-time version of the Goddard Profiling (GPROF) algorithm (Kummerow et al., 1996) applied to TMI data (TRMM product 2A12RT). The intercalibration for the various passive microwave (PMW) estimates is carried out with histogram matching for large global regions that are specific to each data source. Thereafter, the PMW data are merged in 3-hourly windows centered on the nominal observation time.

The second step in the TMPA is to calibrate infrared (IR) brightness temperatures with the combined PMW estimates. This is done with histogram matching for overlapping $3^\circ \times 3^\circ$ squares for roughly 30 days of data to ensure stability. The scheme assumes that colder clouds precipitate more, which is not necessarily true for instantaneous estimates, but yields correct averages for larger scales. There is a fallback scheme that continues to provide (reduced quality) calibration coefficients in cases where the microwave estimates fail, mostly over snowy/frozen land and sea ice. Thereafter, the PMW and IR estimates are combined by using the IR to fill gaps in the PMW for each 3-hourly image. Finally, the multi-satellite field is adjusted to reduce bias. In the production 3B42, this is done using the monthly GPCP Monitoring gauge analyses. For each grid box, all of the combined satellite estimates for the month are summed to create a monthly

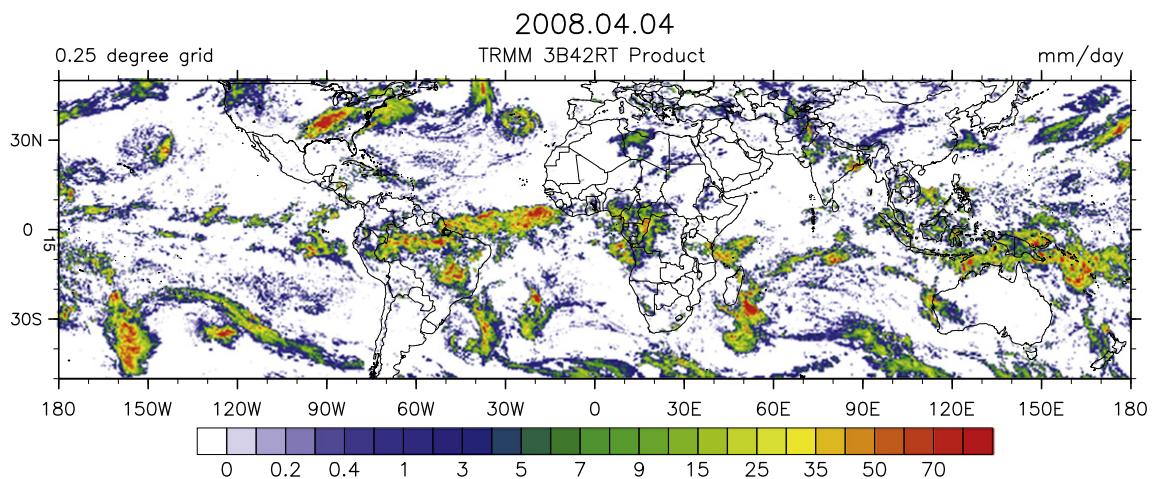


Fig. 8. A sample of daily precipitation estimates (TRMM 3B42RT product). A year worth of data is available as a video in the supplementary information section.

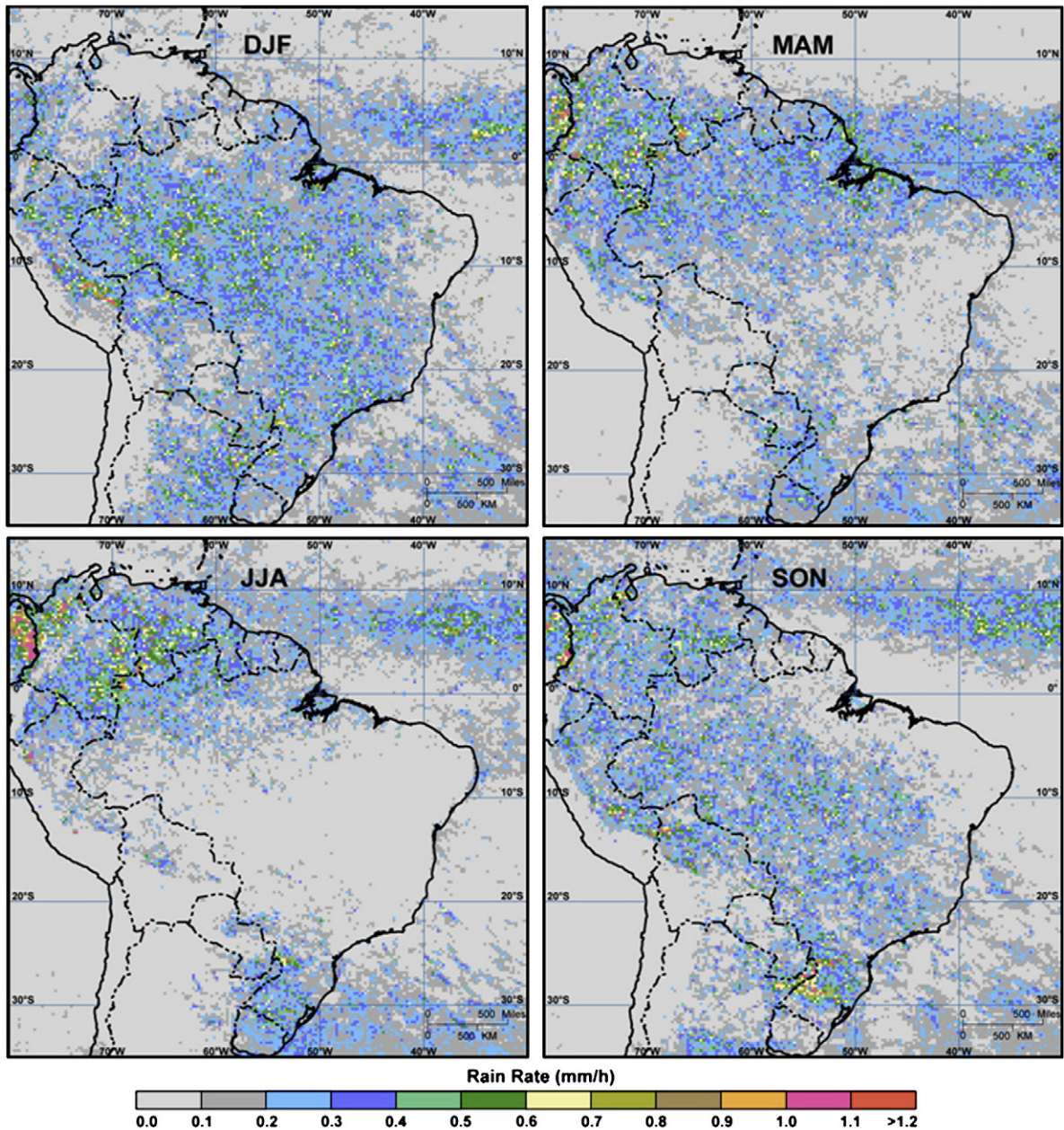


Fig. 9. South America seasonal precipitation estimates (1998–2000) as derived from 3-hourly TRMM data.

multi-satellite estimate. This monthly multi-satellite and the gauge analysis are combined with an inverse random error variance weighting to create TRMM product 3B43, then all the individual 3-hourly combined PWM-IR fields are scaled to sum to the gridbox values of 3B43 and output as TRMM product 3B42. This gives the products the large-area bias of the wind-corrected gauge analysis, with minimal dependence on the gauge analysis where gauges are not present. In the real-time 3B42RT product (Fig. 8), the adjustment is a monthly climatological two-step adjustment, first to the TRMM Combined Instrument (2B31), and then to 3B43 (Huffman et al., 2010). Those products are the basic input of

seasonal accumulations, which are useful for climate or natural risk assessment studies (Fig. 9).

5.2. Model datasets

The second group of precipitation datasets consists in those build upon computer models. These include reanalyses, which explicitly include observations; General Circulation (or Global Climate, depending on context) Models (GCMs) used for climate research and that may or may not include observations; and Regional Climate Models, which in terms of

Table 5
Atmospheric reanalyses comparison table, from NOAA's Reanalysis Intercomparison and Observations (RIO) initiative, <http://reanalyses.org/atmosphere/comparison-table>.

Reanalysis datasets						
Name	Assim. type	Model resolution	Model output resolution	Time coverage	Producer [URL]	
Arctic System Reanalysis (ASR)	WRF-V ar	10–20 km	10–30 km	2000–2010	Polar Met. Group [1]	
ECMWF Interim Reanalysis (ERA Interim)	4D-VAR	T255 I60	125 km	1979–present	ECMWF [2]	
ECMWF 40 year Reanalysis (ERA-40)	3D-VAR	T159 I60	80 km	1958–2001	ECMWF [3]	
Japanese Reanalysis (JRA-25)	3D-VAR	T106 I40	1.125° × 1.125° and 2.5° × 2.5°	1979–2004	Japan Met. Agency [4]	
NASA MERRA	3D-VAR	0.5° × 0.5°	0.5° × 0.5°	1979–2010	NASA [5]	
NCEP Climate Forecast System Reanalysis (CFSR)	3D-VAR	T382 I64	0.5° × 0.5° and 2.5 × 2.5	1979–2010	NCEP [6]	
NCEP/DOE Reanalysis AMIP-II (R2)	3D-VAR	T62 L28	2.5° × 2.5°	1979–present	NCEP/DOE [7]	
NCEP/NCAR Reanalysis I (R1)	3D-VAR	T62 L28	2.5° × 2.5° and 2° × 2° Gauss.	1948–present	NCEP/NCAR [8]	
NCEP North American Regional Reanalysis (NARR)	RDAS	32 km	32 km	1979–present	NCEP [9]	
NOAA-CIRES 20th Century Reanalysis (20CR)	EKF	T62 L28	2° × 2°	1871–2008	NOAA/ESRL PSD [10]	

[1] <http://polarmet.osu.edu/PolarMet/ASR.html>.

[2] <http://www.ecmwf.int/research/era/do/get/era-interim>.

[3] <http://www.ecmwf.int/research/era/do/get/era-interim>.

[4] <http://jra.kishou.go.jp/>.

[5] <http://gmao.gsfc.nasa.gov/research/merra/>.

[6] <http://cfs.ncep.noaa.gov/cfsr/>.

[7] <http://www.cpc.nraa.gov/products/wesley/reanalysis2/>.

[8] <http://www.cpc.nraa.gov/products/wesley/reanalysis.html>.

[9] <http://www.emc.ncep.noaa.gov/mmb/rrean/>.

[10] http://www.esrl.noaa.gov/psd/data/20thC_Rean/.

embedded observational data inherit the properties of the GCMs or reanalysis used for nesting.

5.3. Global Climate Models (GCMs)

The new standard reference database for GCM output is the CMIP5 archive, a follow-on to several Climate Model Intercomparison Programs (CMIP). In the current CMIP5, the Working Group on Coupled Modeling (WGCM) within the World Climate Research Program (WCRP) is promoting a set of climate model experiments, aiming to be the basis of the Intergovernmental Panel on Climate Change (IPCC) Fifth Assessment Report (AR5). Presently, both present-climate and future-climate simulations are been carried out by a number of international groups. An advantage of the coordinated approach is standardized outputs that will make the results more readily comparable and thus less prone to potential errors in the codes.

Several of the intended decadal hindcasts experiments are directly comparable with observational data. These will also be used to verify the models' ability to simulate the present climate, a prerequisite to trust any future-climate simulation. Simulations for near-future climates (up to 2035) under several assumptions in the form of socioeconomic scenarios are important for a continuous monitoring of ongoing global warming, while long-term (2100 onwards) within CMIP5 will serve to ascertain the most likely effects on increasing greenhouse emissions when the effects are clearly seen in the simulations, and well beyond uncertainty limits.

5.3.1. Reanalyses

Datasets of reanalyses such as NCEP's NCEP-2 (Kalnay et al., 1996), CFSR (NCEP's), ERA40 (ECMWF) (Uppala et al., 2005), ERA-interim (ECMWF's, extensively described in Dee et al. (2011), JRA-25 (Japan Meteorological Agency) (Onogi et al., 2007) or MERRA (NASA's Global Modeling and Assimilation Office) (Bosilovich, 2009) provide global data useful for RCM downscaling and for comparison with observational databases. Table 5 gathers the relevant characteristics and links of these datasets. A comparison of the differential characteristics of those reanalysis is summarized below.

NCEP-2 (from 1979 to present day) has a grid resolution of approximately 210 km and does not use some satellite sources such as the SSM/I data. The CFSR (1979–present), a NCEP-2 reanalysis follow-up, has a horizontal resolution of about 38 km, whereas ERA-40 (1957–2002) has a resolution of about 120 km. ERA-40 does not assimilate precipitation, while ERA-interim (1989–present) does but over ocean only, as microwave sensor retrievals over land are highly affected by soil emissivity and thus deemed as unreliable. The JRA-25 (125 km, 1979–present) correlates better with precipitation observations than NCEP-2 and ERA-40 (Bosilovich, 2009), probably due to the assimilation of retrievals from Terra and Aqua satellites and the QuikSCAT instrument. CFSR, on the other hand, assimilates radiances and uses a fully coupled modeling strategy (ocean – including sea ice – and land processes).

In terms of vertical resolution, MERRA (50 km, 1979–present) has 72 vertical levels, which compares to 28 in NCEP-2, 64 in CFSR, 60 in ERA-40 and ERA-Interim, and 40 in JRA-25. ERA-Interim uses 4D variational assimilation, compared to 3D in the others, and seems to have reduced the ERA-40 problem

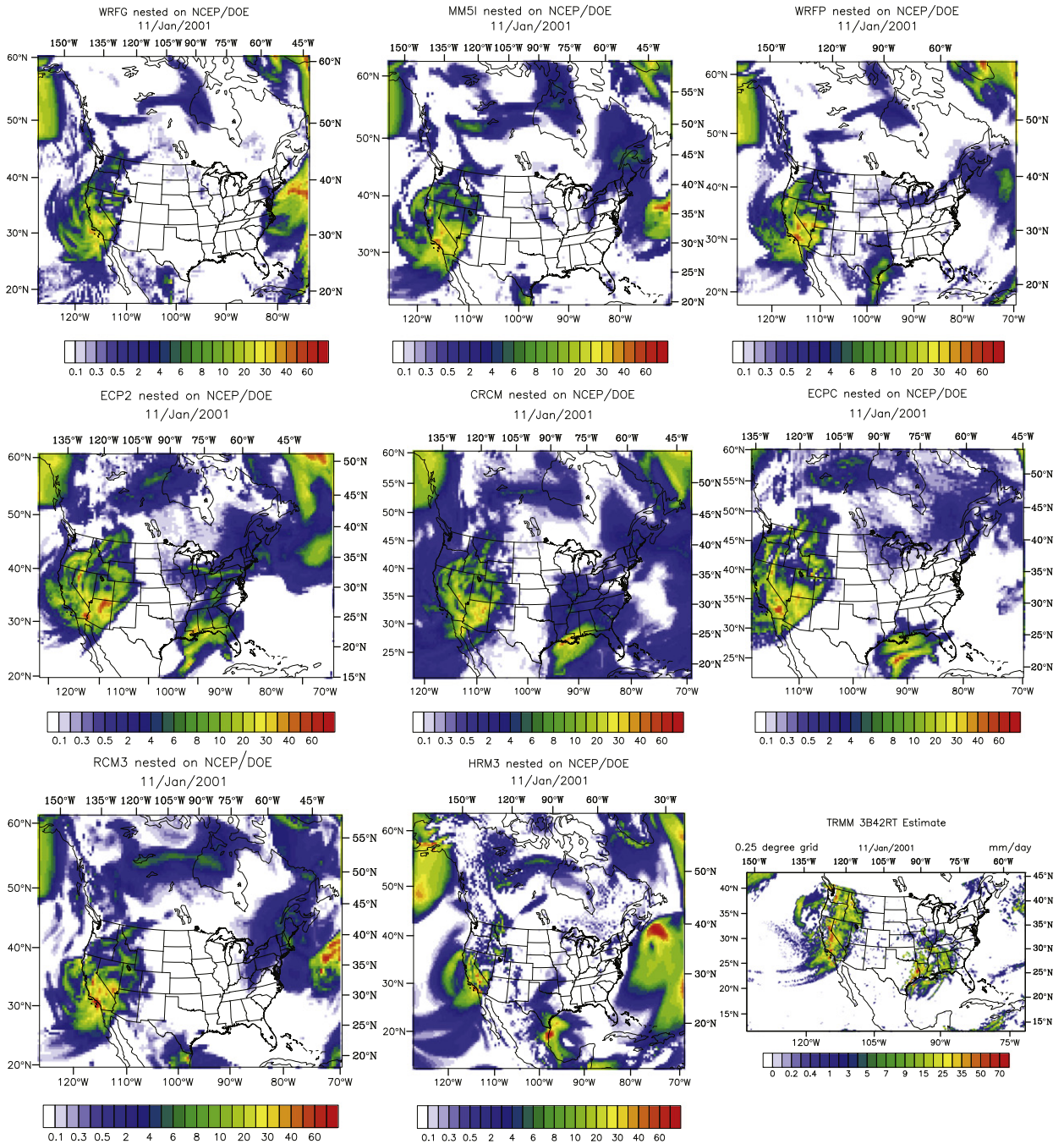


Fig. 10. Sample output of a NARCCAP present-climate experiment. Daily precipitation from several RCMs forced with reanalysis (NCEP/DOE) for Jan 11, 2001. Note that the simulation domains and grids differ. TRMM 3B42RT estimates (up to 50N latitude) included as a reference.

of excess precipitation in the tropics after 1991. Other reanalysis initiatives, such as the one derived from the Japanese Earth Simulator does not currently deliver precipitation fields. The AGCM for the Earth Simulator 2 (AFES 2, Enomoto et al., 2008) is an experiment run at a resolution of about 80 km in the horizontal, with 48 layers in the vertical, and using an ensemble of 40 members over about two years worth of data.

AFES assimilated some observational data (although not satellite radiances) through a local ensemble transform

Kalman filter, and presents the novelty over single GCM runs of providing the spread of the ensemble in addition to the mean values. Such improvements occur at the expense of reducing the temporal span of the simulations.

5.4. Databases of Regional Climate Models

Publicly available databases for research include the results of the EU project PRUDENCE (Christensen and Christensen, 2007),

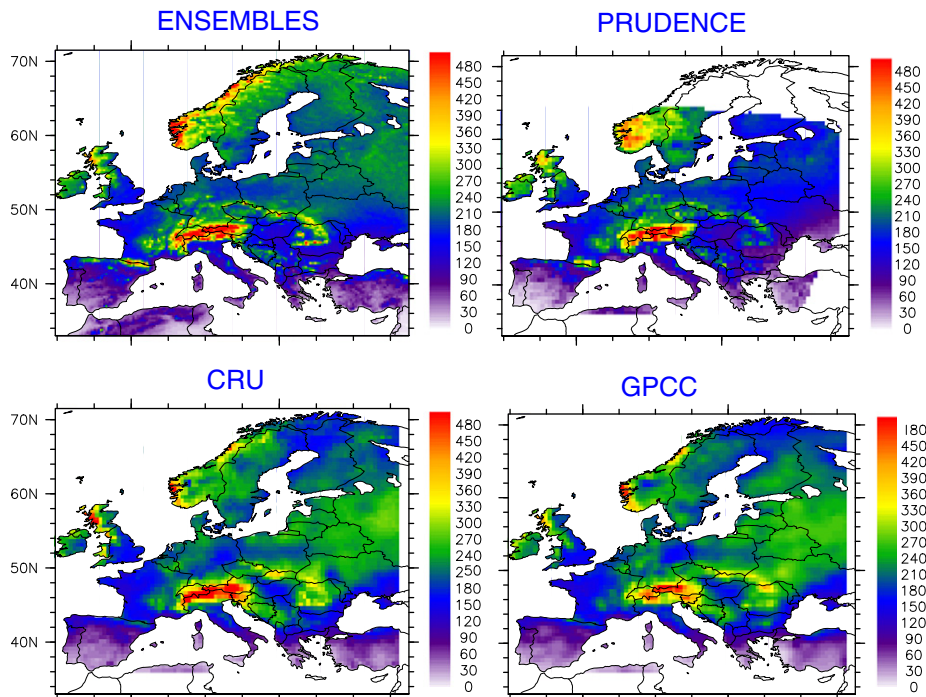


Fig. 11. Summer (JJA) precipitation climatologies as derived by two ensembles of RCMs, ENSEMBLES project (25 km grid size) and PRUDENCE project (50 km grid size), compared with two observational databases, CRU and GPCC. ENSEMBLES RCMs are nested on ERA40 whereas PRUDENCE models are nested on a GCM. Units are mm/season.

where RCMs were nested in GCMs. PRUDENCE was an effort to establish uncertainty limits in climate modeling, providing high-resolution (50 km) estimates from present (1961–1990) and future (2071–2100) climate. The models in the project were quite heterogeneous and included hydrostatic and non-hydrostatic models, with very different parameterizations. Even so, the simulations compare well with observations, especially in terms of aggregated statistics such as model average.

PRUDENCE results were used as a part of the 2007 IPCC scientific report. As in the case of GCMs, the widespread dissemination of IPCC assessments have galvanized the efforts of the climate community, and is driving the efforts of the community to fulfill the needs arising from the reports.

The ENSEMBLES project went a step forward by increasing the spatial resolution to 25 km and by including nesting on the ERA-40 reanalysis (van der Linden and Mitchell, 2009). Comparison of PRUDENCE and ENSEMBLES climates shows that both approaches are consistent but that large uncertainties still remain, specially in the case of precipitation modeling.

The North American Regional Climate Change Assessment Program (NARCCAP; Mearns et al., 2007, 2009), can be seen as the counterpart of European RCM efforts, also nesting RCMs in a reanalysis, the 1979–2004 NCEP/DOE-Reanalysis (Fig. 10).

In order to complete the global picture and to fill the geographical gaps, the CORDEX initiative seeks now to combine these and other RCM efforts such as the CLARIS project (Menéndez et al., 2010) and generate a global land RCM estimate of present and future climates. CORDEX also has a specific focus on providing input for the AR5. While the grid

spacing of the intended CORDEX runs is quite coarse (about 50 km; 10 km for Europe) compared with ERA-interim (about 79 km), nesting on GCM simulations of future climate CMIP5 simulation will allow the generation of an estimate of global precipitation patterns at regional scale for at least one climate change scenario.

6. Applications of global precipitation measurements

The applications of global precipitation measurement span from direct application of the databases to their use as input of tailored models such as those to estimate local water use and allocation in a global warming scenario. As examples, three very different applications are presented: hydropower assessment, data assimilation and validation of regional climate models.

6.1. Hydropower

Hydropower is viewed as the basis of the energy mix sought by policy makers to respond to both growing energy needs and to increasing environmental concerns. Regarding the former, it has been argued that there are no technological limitations for wind, water and solar technologies (referred to as WWS) meeting the world's energy demands by 2030. Within this WWS smart mix, hydropower would play a central role: contrary to other more intermittent renewable technologies such as wind and solar power, hydropower can easily be adjusted to satisfy power demand by simply switching the flow on or off through the penstocks. Hydroelectricity currently represents 86% of total renewable energy

production worldwide (equivalent to 16% of total energy production). China is the largest producer (14.3%), followed by Brazil (12.3%), Canada (12.2%), the US (8.3%), and Russia (5.8%). Some countries, most notably in Central America, virtually rely on hydropower for all their energy needs, making precipitation climatologies much more important to understand and quantify.

The usefulness of the estimates of precipitation from both observation systems and models to hydropower has been recently explored by Tapiador et al. (2011). In terms of daily operations, satellite data can assist to adapt the production to the demand, optimizing the operations. Here, outputs such as those shown in Fig. 8 can be used as inputs for hydrological models. In the long term, simulations of future precipitation are useful to planning new installations, since climate change may adversely affect the financial viability of both existing and potential hydropower. Within this area, a knowledge of not only rainfall amounts but also cycles is fundamental: changes in river regimes in the future climate may result in oversized or undersized plants. Regional studies of the effects of climate change on the hydropower potential have been carried out for Europe (Lehner et al., 2005) illustrating the need for informed knowledge about changes in future precipitation.

Regarding climate modeling, policy consequences in terms of planning and sizing resources can be derived drawing on the outcomes of RCMs. This has to be done within the uncertainty limits of the projections, most of which are derived from comparing with observations. Therefore, constructing reliable present-climate climatologies is crucial to informed decisions in this area. It has to be noted that the hydropower potential is still well above the current installed capacity in all regions, except Europe which has already achieved high capacity. A threefold increase is believed to be possible in Asia and Africa, and there is room to more than double the capacity in North America, Africa and Latin America.

6.2. Data assimilation into NWP models

Numerical Weather Prediction (NWP) is an initial-boundary value problem. With a given estimate of the state of the atmosphere (initial conditions) and lateral boundary conditions, the model simulates the atmospheric evolution. Obtaining these initial conditions is a very important and complex issue and has become a science itself (Daley, 1996). In NWP, a previous short-range forecast is the starting point to obtain a first guess of the initial state of the atmosphere, and here the use of observations considerably improves the performances of the model. It is within this aspect that precipitation plays a central role.

Data assimilation is the process through which real observations are added to the initial conditions of the model, thus improving the background of the first guess. The observations come from different instruments at different locations and times and must be decoded and assembled for use into the assimilation system. Not all types of observations are assimilated in the same way. Thus for example, cloudy conditions may affect suitable satellite radiance data but clouds may allow for satellite cloud-track wind data at cloud top.

Analysis increments are obtained as the weighted difference between the observations and the model first guess.

Objective analysis procedures are used to obtain the analysis increments, as a result of changes applied to the first guess fields taking into account the effect of all observations. Here, precipitation information helps to nudge the model towards a more realistic state. The weight factor can be determined from estimated statistical error covariances of both, forecast and observations (Kalnay, 2003) using several possible schemes.

The background error covariance matrix is the way to spread the information to those grid points and model variables that are not used explicitly to formulate the observation operator. Bergthorsson and Döös (1955), Cressman (1959), and Barnes (1964) have used different correction methods (SCM) to obtain weights empirically as functions of the distance between observations and grid points. The Optimal Interpolation (OI) scheme was applied by Gandin (1963) and became the standard operational analysis scheme during the 1980s and 1990s.

Precipitation can also be assimilated into 3D or 4D schemes. The three-dimensional variational data assimilation procedure (3DVAR) (Parrish and Derber, 1992; Courtier et al., 1998; Gauthier et al., 1998; Cohn et al., 1998) is equivalent to the OI scheme, although the method for solving it is quite different. 3DVAR allows nonlinearity in the relationship between observed quantities and analysis variables. Several weather forecast services have implemented this procedure for their operational forecasts, among others the National Center for Environmental Prediction (NCEP) (Parrish and Derber, 1992) and the ECMWF (Courtier et al., 1998).

The main limitation of standard 3DVAR is that it spreads the influence of observations following an isotropic scheme for each weather situation, regardless of the presence of fronts, stable layers or any other features. The scheme was reformulated to define the analysis increments on the vertical coordinate of the model and to provide a new view of the background error covariances (Gauthier et al., 1999). The concept of 'anisotropic background error covariances' was then introduced as a different set of assumptions that control the influence pattern that an observation increment can have on the analysis.

Talagrand and Courtier (1987) demonstrated that the use of the adjoint of a numerical model enables us to obtain the initial conditions leading to a forecast that would best fit data available over a finite time interval. A four-dimensional variational data assimilation formulation (4DVAR, Le Dimet and Talagrand, 1986; Lewis and Derber, 1985; Talagrand and Courtier, 1987; Courtier and Talagrand, 1987) makes use of this result extending 3DVAR in the time dimension. 4DVAR improves the integration of all variables, including vertical motion, clouds and precipitation. This system also makes a better use of more observations from the same sites, including observations from geostationary satellites. 4DVAR has been used in different models with subsequent and sophisticated physical parameterizations (Zou and Kuo, 1996; Zou, 1997; Tsuyuki, 1997; Zupanski and Mesinger, 1995; Zupanski, 1993; Mahfouf et al., 2000). This approach has been used in the context of an operational environment at the European Centre for Medium-Range Weather Forecasts (ECMWF) since 1997 (Rabier et al., 2000) or at Meteo-France since 2000 (Gauthier and Thépaut, 2001), the Japan Meteorological Agency in 2002

(Ishikawa and Koizumi, 2002) or the Met Office in 2004 (Collard, 2004).

A more efficient alternative to 3DVAR or 4DVAR to assimilate precipitation is the Kalman filtering method. The forecast error covariance is computed using the forecast model itself (Kalnay, 2003). The covariance patterns are statistically estimated using ensemble forecasts and require a high computational power.

The Ensemble Kalman Filter (EKF) combines an ensemble forecast and a data assimilation system. The process begins with an ensemble of analyses and an ensemble of short-range forecasts to the time of the next observations available. The different ensemble members are used to estimate the forecast covariances required to assimilate the new observations. The new observations obtained by assimilating a set of perturbed observations then provide a new scenario (Houtekamer et al., 1996; Houtekamer and Mitchell, 1998, 2001; Hamill and Snyder, 2000; Hamill et al., 2001; Anderson, 2001).

6.3. RCM validation

In climate applications, there is also a need for better precipitation estimates, which are used as validation data. While it is acknowledged that a good match with observations in present climate does not guarantee model performance in future climates, successful control runs are a prerequisite to trust any model. Thus, modelers use present-day climatologies to gauge the model ability to capture important processes such as convection and cloud microphysics.

Satellite precipitation data can assist to this validation/verification task. Fig. 11 shows the results of one such validations. The present-climate simulations of eleven regional climate models involved in the EU PRUDENCE and ENSEMBLES projects are here compared with rain gauge observations (CRU and GPCC). The match of the ensemble mean is good enough to place confidence in the performances in future climates under the assumption that the same processes and feedbacks that operate in the present climate will operate in the same way in the future.

For climatological uses, the availability of long series (typically 30 years) of data is a requirement, but shorter periods have been found also useful to validate the models. Thus, thanks to satellite data it has been shown that RCMs provide consistent estimates of precipitation after accounting for known uncertainties in the reference data (Tapiador, 2010). Gauge and satellite-merged data (CRU, GPCP, CMAP, CPC, and GPCC databases) have compared with RCMs simulations over Europe both in terms spatially reproducing the climatology and the *pdfs* of precipitation (Tapiador, 2009), and in terms of capturing the phase and power of precipitation cycles (Tapiador and Sanchez, 2008), obtaining consistent results. These topics are fertile research ground, as a good match within uncertainties between models and observations builds confidence in models been capable of simulating the climates of the future.

7. Outlook

Precipitation is a meteorological variable that is difficult to measure precisely (Levizzani et al., 2007; Anagnostou et

al., 1999). Disdrometers, scanners, radars and radiometers present their own sources of error, limitations and uncertainties. This results in a challenge for those aiming to provide a timely and precise estimate of how much precipitation reaches the ground, and in which state (solid, liquid, or mixed).

Large international projects such as the Global Precipitation Measurement (GPM) mission seek advances in this field. The GPM mission will be highly relevant for hydrological applications as it will be provide, for the first time, adequate sampling of precipitation in middle to high latitudes using an orbital radar. The mission will provide global retrievals of precipitation, with a goal of 3-hour revisit over land owing to the mixed non-sun-synchronous/sun-synchronous orbits of the constellation members including the MW sounders. This configuration will expand the TRMM capability for physically direct sensing of precipitation to higher latitudes.

Currently at issue is the optimum combination of measurements, estimates and model outputs to reinforce the individual strengths and address the shortcomings to providing a better understanding of precipitation. While the performance of most NWP models lags behind satellite algorithms in estimating current precipitation, only models can give the estimates of future precipitation.

Regarding climate, observational databases are routinely used to fine-tuning RCMs parameterizations, whereas GCMs and RCMs can provide insight into changes in the immediate future to applications currently using those databases, such as agriculture, hydropower, or water resource management. Within the precipitation science umbrella, cross-fertilization between different branches can only help each other.

Supplementary materials related to this article can be found online at [doi:10.1016/j.atmosres.2011.10.021](https://doi.org/10.1016/j.atmosres.2011.10.021).

Acknowledgements

The work of FTJ (Tapiador) has been funded through projects CGL2010-20787-C02-01, CGL2010-20787-C02-02, CENIT PROMETEO (MICCIN), and PPII10-0162-554 (JCCM). The contributions from FJT (Turk) were performed at the Jet Propulsion Laboratory, California Institute of Technology, under contract with the National Aeronautics and Space Administration. EGO acknowledges research project LE176A11-2 (JCyL). GJH and WP acknowledge the NASA PMM (Dr. Ramesh Kakar) and GPM Programs for funding support. FJT (Tapiador), FJT (Turk), WP, AYH, LATM, CFA, PS, and GJH are current Principal Investigators in the Precipitation Measurement Missions (PMM, GPM + TRMM) science team. PRUDENCE project was funded by the EU FP5 (Contract no. EVK2-CT-2001-00132). The ENSEMBLES data used in this work was funded by the EU FP6 (Contract no. 505539). NAR-CAPP is funded by the DoE, EPA, NOAA and NSF. The CMAP, CPC, CRU, GPCC, GPCP and TRMM data providers are also gratefully acknowledged.

References

- Adler, R.F., Negri, A.J., 1988. A satellite infrared technique to estimate tropical convective and stratiform rainfall. *J. Appl. Meteorol.* 27, 30–51.
- Adler, R.F., Negri, A.J., Keehn, P.R., Hakkarinen, I.M., 1993. Estimation of monthly rainfall over Japan and surrounding waters from a combination

- of low-orbit microwave and geosynchronous IR data. *J. Appl. Meteorol.* 32, 335–356.
- Adler, Robert F., et al., 2003. The version-2 Global Precipitation Climatology Project (GPCP) monthly precipitation analysis (1979–present). *J. Hydrometeorol.* 4, 1147–1167.
- Amitai, E., Petersen, W.A., Llort, X., Vasilof, S., 2011. Multi-platform comparisons of rain intensity for extreme precipitation events. *IEEE Trans. Geosci. Remote Sens.* 99, 1–12.
- Anagnostou, E.N., Krajewski, W., Smith, J., 1999. Uncertainty quantification of mean-areal radar rainfall estimates. *J. Atmos. Oceanic Technol.* 16, 206–215.
- Anderson, J.L., 2001. An ensemble adjustment filter for data assimilation. *Mon. Weather Rev.* 129, 2884–2903.
- Arkin, P.A., Meisner, B.N., 1987. The relationship between large-scale convective rainfall and cold cloud over the western hemisphere during 1982–84. *Mon. Weather Rev.* 115, 51–74.
- Barnes, S., 1964. A technique for maximizing details in numerical map analysis. *J. Appl. Meteorol.* 3, 395–409.
- Barrett, E.C., Kidd, C., Bailey, J.O., 1987. The use of SMMR data in support of the Bristol/NOAA Interactive Scheme (BIAS) for satellite-improved rainfall monitoring. Annual report to the US Department of Commerce, contract No. NA86AA-H-RA001, Washington D.C. 77 pp.
- Beck, C., Grieser, J., Rudolf, B., 2004. A New Monthly Precipitation Climatology for the Global Land Areas for the Period 1951 to 2000. German Weather Service Climate Status Rep., Offenbach, Germany, pp. 181–190.
- Behrangi, A., Iman, B., Hsu, K.-L., Sorooshian, S., Bellerby, T.J., Huffman, G.J., 2010. REFAME: Rain Estimation using Forward-adjusted Advection of Microwave Estimates. *J. Hydrometeorol.* 11, 1305–1321.
- Bellerby, T., 2006. High-resolution 2D cloud-top advection from geostationary satellite imagery. *IEEE Trans. Geosci. Remote Sens.* 44, 3639–3648.
- Bergthorsson, P., Döös, B.R., 1955. Numerical weather map analysis. *Tellus* 7, 329.
- Bosilovich, M., 2009. NASA's Modern Era Retrospective—Analysis for Research and Applications (MERRA). Presentation to the Department of Earth and Atmospheric Sciences, Purdue University, Sept 24, 2009.
- Brandes, E.A., Ikeda, K., Zhang, G., 2007. A statistical and physical description of hydrometeor distributions in Colorado snowstorms using a video disdrometer. *J. Appl. Meteorol. Climatol.* 46, 634–650.
- Briggs, P.R., Cogley, J.G., 1996. Topographic bias in mesoscale precipitation networks. *J. Climate* 9, 205–218.
- Bringi, V.N., Chandrasekar, V., 2001. Polarimetric Doppler Weather Radar: Principles and Applications. Cambridge University Press. 636 pp.
- Bringi, V.N., et al., 2003. Raindrop size distribution in different climatic regimes from disdrometer and dual-polarized radar analysis. *J. Atmos. Sci.* 60, 354–365.
- Bringi, V.N., Williams, C.R., Thurai, M., May, P.T., 2009. Using dual-polarized radar and dual-frequency profiler for dsd characterization: a case study from Darwin, Australia. *J. Atmos. Oceanic Technol.* 26, 2107–2122.
- Cao, Q., Zhang, G., Brandes, E., Schuur, T., Ryzhkov, A., Ikeda, K., 2008. Analysis of video disdrometer and polarimetric radar data to characterize rain microphysics in Oklahoma. *J. Appl. Meteorol. Climatol.* 47, 2238–2255.
- Chandrasekar, V., Hou, A., Smith, E., Bringi, V.N., Rutledge, S.A., Gorgucci, E., Petersen, W.A., 2008. Use of dual polarization radars for validation of spaceborne precipitation measurements: rationale and opportunities. *Bull. Amer. Meteorol. Soc.* 89, 1127–1145.
- Chang, W.-Y., Wang, T.-C., Lin, P.-L., 2009. Characteristics of the raindrop size distribution and drop shape relation in typhoon systems in the western Pacific from the 2D video disdrometer and NCU C-band polarimetric radar. *J. Atmos. Oceanic Technol.* 26, 1973–1993.
- Chen, M., Xie, P., Janowiak, J.E., Arkin, P.A., 2002. Global land precipitation: a 50-yr monthly analysis based on gauge observations. *J. Hydrometeorol.* 3, 249–266.
- Chiu, L., Chang, A., Janowiak, J.E., 1993. Comparison of monthly rain rates derived from GPI and SSM/I using probability distribution functions. *J. Appl. Meteorol.* 32, 323–334.
- Christensen, J.H., Christensen, O.B., 2007. A summary of the PRUDENCE model projections of changes in European climate by the end of this century. *Clim. Chang.* 81, 7–30.
- Ciach, G.J., 2003. Local random errors in tipping-bucket rain gauge measurements. *J. Atmos. Oceanic Technol.* 20, 752–759.
- Ciach, G.J., Krajewski, W.F., 2006. Analysis and modeling of spatial correlation structure in small-scale rainfall in Central Oklahoma. *Adv. Water Res.* 29, 1450–1463.
- Cohn, S.E., da Silva, D.M., Guo, J., Sienkiewicz, M., Lamich, D., 1998. Assessing the effects of data selection with the DAO physical space statistical analysis system. *Mon. Weather Rev.* 126, 2913–2926.
- Collard, A.D., 2004. Assimilation of AIRS observations at the Met Office. Proc. of the ECMWF workshop on assimilation of high spectral resolution sounders in NWP, pp. 63–71.
- Courtier, P., Talagrand, O., 1987. Variational assimilation of meteorological observations with the adjoint vorticity equation. Part II: numerical results. *Q. J. R. Meteorol. Soc.* 113, 1129–1347.
- Courtier, P., Andersson, P.E., Heckley, W., Pailleux, J., Vasiljevic, D., Hamrud, M., Hollingsworth, A., Rabier, F., Fisher, M., 1998. The ECMWF implementation of three-dimensional variational assimilation (3D-Var). I: formulation. *Q. J. R. Meteorol. Soc.* 124, 1783–1807.
- Cressman, G.P., 1959. An operational objective analysis system. *Mon. Weather Rev.* 87, 367–374.
- Daley, R., 1996. Atmospheric Data Analysis. Cambridge University Press. 457 pp.
- Dee, D.P., Uppala, S.M., Simmons, A.J., Berrisford, P., Poli, P., Kobayashi, S., Andrae, U., Balmaseda, M.A., Balsamo, G., Bauer, P., Bechtold, P., Beljaars, A.C.M., van de Berg, L., Bidlot, J., Bormann, N., Delsol, C., Dragani, R., Fuentes, M., Geer, A.J., Haimberger, L., Healy, S.B., Hersbach, H., Holm, E.V., Isaksen, I., Kallberg, P., Kihler, M., Matricardi, M., McNally, A.P., Monge-Sanz, B.M., Morcrette, J.-J., Park, B.-K., Peubey, C., de Rosnay, P., Tavolato, C., Thepaut, J.-N., Vitart, F., 2011. The ERA-Interim reanalysis: configuration and performance of the data assimilation system. *Q. J. R. Meteorol. Soc.* 137, 553–597.
- Ebert, E.E., 2007. Methods for verifying satellite precipitation estimates. In: Levizzani, V., et al. (Ed.), *Measuring Precipitation from Space, EURAINSAT and the future*. Springer, pp. 345–356.
- Ebert, E.E., Janowiak, J.E., Kidd, C., 2007. Comparison of near-real-time precipitation estimates from satellite observations and numerical models. *Bull. Am. Meteorol. Soc.* 88, 47–64.
- Elsaesser, G.S., Kummerow, C., 2008. Toward a fully parametric retrieval of the nonraining parameters over the global oceans. *J. Appl. Meteorol.* 47, 1599–1618.
- Enomoto, T., Kuwano-Yoshida, A., Komori, N., Ohfuchi, W., 2008. Description of AFES 2: improvements for high-resolution and coupled simulations. In: Hamilton, K., Ohfuchi, W. (Eds.), *High Resolution Numerical Modelling of the Atmosphere and Ocean*. Springer, New York, pp. 77–97. chapter 5.
- Gandin, L.S., 1963. Objective Analysis of Meteorological Fields. GIMIZ, Leningrad.
- García-Ortega, E., Fita, L., Romero, R., López, L., Ramis, C., Sánchez, J.L., 2005. Numerical simulation and sensitivity study of a severe hailstorm in northeast Spain. *Atmos. Res.* 83 (2–4).
- García-Ortega, E., López, L., Sánchez, J.L., Marcos, J.L., 2006. Microphysical analysis at the cloud edge of a severe hailstorm. *Atmos. Res.* 82 (1–2).
- García-Ortega, E., López, L., Sánchez, J.L., 2011. Atmospheric patterns associated with hailstorm days in the Ebro Valley, Spain. *Atmos. Res.* 100, 401–427.
- Gauthier, P., Thépaut, J.-N., 2001. Impact of the digital filter as a weak constraint in the preoperational 4DVAR assimilation system of Météo-France. *Mon. Weather Rev.* 129, 2089–2102.
- Gauthier, P.C., Charette, L., Fillion, L., Koclas, P., Laroche, S., 1998. Implementation of a 3D variational data assimilation system at the Canadian Meteorological Center. Part I: the global analysis. *Atmos. Ocean* 37, 103–156.
- Gauthier, P.C., Buehner, M., Fillion, L., 1999. Background-error statistics modelling in a 3D variational data assimilation scheme: estimation and impact on the analyses. *Proc. ECMWF Workshop on Diagnosis of Data Assimilation Systems*, Reading, United Kingdom, ECMWF, pp. 131–145.
- Giorgi, F., Marinucci, M.R., Visconti, G., 1990. Use of a limited-area model nested in a general-circulation model for regional climate simulation over Europe. *J. Geophys. Res.-Atmos.* 95 (D11), 18413–18431.
- Greco, M., Olson, W.S., Anagnostou, E., 2004. Retrieval of precipitation profiles from multiresolution, multifrequency, active and passive microwave radar observations. *J. Appl. Meteorol.* 43, 562–575.
- Gunn, R., Kinze, G., 1949. The terminal velocity of fall for water droplets in stagnant air. *J. Meteorol.* 6, 243–248.
- Habib, E., Krajewski, W.F., 2002. Uncertainty analysis of the TRMM ground-validation radar-rainfall products: application to the TEFLUN-B field campaign. *J. Appl. Meteorol.* 41, 558–572.
- Habib, E., Krajewski, J.W.F., Kruger, A., 2001. Sampling errors of tipping-bucket rain gauge measurements. *J. Hydrol. Eng.* 159–166 (March–April).
- Haddad, Z.S., Short, D.A., Durden, S.L., Im, E., Hensley, S., Grable, M.B., Black, M.B., 1997a. A new parameterization of the rain drop size distribution. *IEEE Trans. Geosci. Remote Sens.* 35, 532–539.
- Haddad, Z.S., Smith, E.A., Kummerow, C.D., Iguchi, T., Farrar, M.R., Durden, S.L., Alves, M., Olson, W.S., 1997b. The TRMM “Day-1” radar/radiometer combined rain-profiling algorithm. *J. Meteorol. Soc. Jpn.* 75, 799–809.
- Hamil, T.M., Snyder, C., 2000. A hybrid ensemble Kalman filter/3d-variational analysis scheme. *Mon. Weather Rev.* 128, 2905–2919.
- Hamil, T.M., Whitaker, J.S., Snyder, C., 2001. Distance-dependent filtering of background-error covariance estimates in an ensemble Kalman filter. *Mon. Weather Rev.* 129, 2776–2790.
- Hong, Y., Hsu, K.-L., Moradkhani, H., Sorooshian, S., 2006. Uncertainty quantification of satellite precipitation estimation and Monte Carlo

- assessment of the error propagation into hydrologic response. *J. Water Res. Res.* 42, W08421. doi:10.1029/2005WR004398.
- Houtekamer, P.L., Mitchell, H.L., 1998. Data assimilation using an ensemble Kalman filter technique. *Mon. Weather Rev.* 126, 796–811.
- Houtekamer, P.L., Mitchell, H.L., 2001. A sequential ensemble Kalman filter for atmospheric data assimilation. *Mon. Weather Rev.* 129, 123–137.
- Houtekamer, P.L., Lefaiivre, L., Derome, J., 1996. The RPN ensemble prediction system. *Proc. ECMWF Seminar on Predictability*, vol. II, pp. 121–146. 4–8 September 1995, Reading, UK.
- Huang, G., Bringi, V.N., Cifelli, R., Hudak, D., Petersen, W., 2010. A methodology to derive radar reflectivity–liquid equivalent snow rate relations using C-band radar and a 2D video disdrometer. *J. Appl. Meteorol.* 27, 637–651.
- Huffman, G.J., et al., 1997. The Global Precipitation Climatology Project (GPCP) combined precipitation dataset. *Bull. Amer. Meteor. Soc.* 78, 5–20.
- Huffman, G.J., Morrissey, M., Bolvin, D.T., Curtis, S., Joyce, R., McGavock, B., Susskind, J., 2001. Global precipitation at one-degree daily resolution from multisatellite observations. *J. Hydrometeorol.* 2, 36–50.
- Huffman, G.J., Adler, R.F., Bolvin, D.T., Gu, G., Nelkin, E.J., Bowman, K.P., Hong, Y., Stocker, E.F., Wolff, D.B., 2007. The TRMM multi-satellite precipitation analysis: quasi-global, multi-year, combined-sensor precipitation estimates at fine scale. *J. Hydrometeorol.* 8, 38–55.
- Huffman, G.J., Adler, R.F., Bolvin, D.T., Nelkin, E.J., 2010. The TRMM Multi-satellite Precipitation Analysis (TMPA). Chapter 1 In: Hossain, F., Gebremichael, M. (Eds.), *Satellite Rainfall Applications for Surface Hydrology*. Springer Verlag. ISBN: 978-90-481-2914-0, pp. 3–22.
- Iguchi, T., Kozu, T., Kwiatkowski, J., Meneghini, R., Awaka, J., Okamoto, K., 2009. Uncertainties in Rain-profiling algorithm for the TRMM precipitation radar. *J. Meteorol. Soc. Jpn.* 87A, 1–30.
- Ishikawa, Y., Koizumi, K., 2002. Meso-scale analysis. *Outline of the Operational Numerical Weather Prediction at the Japan Meteorological Agency*, pp. 26–31.
- Jaffrain, J., Studzinski, A., Berne, A., 2011. A network of disdrometers to quantify the small-scale variability of the raindrop size distribution. *Wat. Res. Res.* 47, W00H06.
- Joss, J., Waldvogel, A., 1967. Ein Spektrograph für Niederschlagstropfen mit automatischer Auswertung. *Pure Appl. Geophys.* 68, 240–246.
- Joyce, R.J., Janowiak, J.E., Arkin, P.A., Xie, P., 2004. CMORPH: a method that produces global precipitation estimates from passive microwave and infrared data at high spatial and temporal resolution. *J. Hydrometeorol.* 5, 487–503.
- Kalnay, E., 2003. *Atmospheric Modeling, Data Assimilation and Predictability*. Cambridge University Press, Cambridge, 330 pp.
- Kalnay, E., Kanamitsu, M., Kistler, R., Collins, W., Deaven, D., Gandin, L., Iredell, M., Saha, S., White, G., Woollen, J., Zhu, Y., Leetmaa, A., Reynolds, R., Chelliah, M., Ebisuzaki, W., Higgins, W., Janowiak, J., Mo, K.C., Ropelewski, C., Wang, J., Jenne, R., Joseph, D., 1996. The NCEP/NCAR 40-year reanalysis project. *Bull. Am. Meteorol. Soc.* 77 (3), 437–471.
- Kidd, C., Kniveton, D.R., Todd, M.C., Bellerby, T.J., 2003. Satellite rainfall estimation using a combined passive microwave and infrared algorithm. *J. Hydrometeorol.* 4, 1088–1104.
- Klein Tank, A.M.G., Wijngaard, J.B., et al., 2002. Daily dataset of 20th-century surface air temperature and precipitation series for the European Climate Assessment. *Int. J. Climatol.* 22, 1441–1453.
- Knollenberg, R.G., 1970. The optical array: an alternative to scattering or extinction for airborne particle size determination. *J. Appl. Meteorol.* 9, 86–103.
- Krajewski, W., 2007. Ground networks: are we doing the right things? In: Levizzani, et al. (Ed.), *Measuring precipitation from space. EURAINSAT and the Future*. Springer, pp. 403–417.
- Krajewski, W.F., Ciach, G.J., Habib, E., 2003. An analysis of small-scale rainfall variability in different climate regimes. *J. Hydrol. Sci.* 48, 151–162.
- Krajewski, W.F., et al., 2006. DEVEX-disdrometer evaluation experiment: basic results and implications for hydrologic studies. *Adv. Water Res.* 29, 311–325.
- Kubota, T., Shige, S., Hashizume, H., Aonashi, K., Takahashi, N., Seto, S., Takayabu, Y.N., Ushio, T., Nakagawa, K., Iwanami, K., Kachi, M., Okamoto, K., 2007. Global precipitation map using satellite-borne microwave radiometers by the GSMaP project: production and validation. *IEEE Trans. Geosci. Remote Sens.* 45, 2259–2275.
- Kummerow, C., 1998. Beamfilling errors in passive microwave rainfall retrievals. *J. Appl. Meteorol.* 37 (4), 356–370.
- Kummerow, C., Olson, W.S., Giglio, L., 1996. A simplified scheme for obtaining precipitation and vertical hydrometeor profiles from passive microwave sensors. *IEEE Trans. Geosci. Remote Sens.* 34, 1213–1232.
- Lanzinger, E., Theel, M., Windolph, H., 2006. Rainfall amount and intensity measured by the Thies laser precipitation monitor, TECO-2006, Geneva, Switzerland.
- Larsen, M.L., Clark, A., Noffke, M., Saltzgeber, G., Steele, A., 2010. Identifying the scaling properties of rainfall accumulation as measured by a rain gauge network. *Atmos. Res.* 96 (1), 149–158.
- Le Dimet, F., Talagrand, O., 1986. Variational algorithms for analysis and assimilation of meteorological observations: theoretic aspects. *Tellus* 38A, 97–110.
- Lehner, B., Czisch, G., Vassolo, S., 2005. The impact of global change on the hydropower potential of Europe: a model-based analysis. *Energy Pol.* 33 (7), 839–855.
- Levizzani, V., Bauer, P., Turk, F.J. (Eds.), 2007. *Measuring Precipitation from Space*. Springer-Verlag, 721 pp.
- Lewis, J., Derber, J., 1985. The use of adjoint equations to solve a variational adjustment problem with advective constraints. *Tellus* 37A, 309–327.
- Liebmann, B., Allured, D., 2005. Daily precipitation grids for South America. *Bull. Amer. Meteor. Soc.* 86, 1567–1570.
- Löffler-Mang, M., Joss, J., 2000. An optical disdrometer for measuring size and velocity of hydrometeors. *J. Atmos. Oceanic Technol.* 17, 130–139.
- Machado, L.A.T., Martins, R.C.G., 2008. Convective cloud characteristics in the southwestern Amazonia during wet and pre wet season. 5th International Conference on Clouds and Precipitation ICCP, Cancun, México.
- Machado, L.A.T., Rossow, W.B., 1993. Structural characteristics and radiative properties of tropical cloud clusters. *Mon. Weather Rev.* 121, 3234–3260.
- Machado, L.A.T., Rossow, W.B., Guedes, R.L., Walker, A., 1998. Life cycle variations of convective systems over the Americas. *Mon. Weather Rev.* 126, 1630–1654.
- Mahfouf, J.-F., Viterbo, P., Douville, H., Beljaars, A.C.M., Saarinen, S., 2000. A revised land-surface analysis scheme in the integrated forecasting system. *ECMWF Newsletter*, No. 88. ECMWF, Reading, United Kingdom, pp. 8–13.
- Maraes-Frasson, R.-P., da Cunha, L.K., Krajewski, W.F., 2011. Assessment of the Thies optical disdrometer performance. *Atmos. Res.* 101, 237–255.
- Mearns, L.O., et al., 2007. Updated 2011. The North American Regional Climate Change Assessment Program Dataset. National Center for Atmospheric Research Earth System Grid data portal, Boulder, CO.
- Mearns, L.O., Gutowski, W.J., Jones, R., Leung, L.-Y., McGinnis, S., Nunes, A.M.B., Qian, Y., 2009. A regional climate change assessment program for North America. *EOS* 90 (36), 311–312 (8 September).
- Menéndez, C.G., de Castro, M., Sorensson, A., Boulanger, J.-P., 2010. CLARIS project: towards climate downscaling in South America. *Meteorol. Z.* 19 (4), 357–362 (6).
- Michaelides, S., Levizzani, V., Anagnostou, E., Bauer, P., Kasparis, T., Lane, J.E., 2009. Precipitation: measurement, remote sensing, climatology and modeling. *Atmos. Res.* 94, 512–533.
- Mirovsky, B.J., Bradley, A.A., Eichinger, W.E., Krajewski, W.F., Kruger, A., Nelson, B.R., Creutin, J.-D., 2004. An experimental study of small-scale variability of radar reflectivity using disdrometer observations. *J. Clim.* 43 (1), 106–118.
- Moore, R.J., Jones, D.A., Cox, D.R., Isham, V.S., 2000. Design of the HYRES rain-gauge network. *Hydrol. Earth Syst. Sci.* 4, 523–530.
- Moreau, E., Testud, J., Le Bouar, E., 2009. Rainfall spatial variability observed by X-band weather radar and its implication for the accuracy of rainfall estimates. *Adv. Water Res.* doi:10.1016/j.advwatres.2008.11.007.
- Morrissey, M.L., Maliekal, J.A., Greene, J.S., Wang, J., 1995. The uncertainty of simple spatial averages using rain gauge networks. *Wat. Res. Res.* 31, 2011–2017.
- Nespor, V., Krajewski, W.F., Kruger, A., 2000. Wind-induced error of raindrop size distribution measurement using a two-dimensional video disdrometer. *J. Atmos. Oceanic Technol.* 17 (11), 1483–1492.
- New, M., Hulme, M., Jones, P., 1999. Representing twentieth century space-time climate variability. Part I: development of a 1961–90 mean monthly terrestrial climatology. *J. Climate* 12, 829–856.
- New, M., Hulme, M., Jones, P., 2000. Representing twentieth-century space-time climate variability. Part II: development of 1901–96 monthly grids of terrestrial surface climate. *J. Climate* 13, 2217–2238.
- Onogi, K., Tsutsui, J., Koide, H., Sakamoto, M., Kobayashi, S., Hatsushika, H., Matsumoto, T., Yamazaki, N., Kamahori, H., Takahashi, K., Kadokura, S., Wada, K., Kato, K., Oyama, R., Ose, T., Mannoji, N., Taira, R., 2007. The JRA-25 reanalysis. *J. Meteorol. Soc. Jpn.* 85, 369–432.
- Parrish, D.F., Derber, J.C., 1992. The National Meteorological Center's spectral statistical interpolation analysis system. *Mon. Weather Rev.* 120, 1747–1763.
- Pedersen, L., Jensen, N.E., Christensen, L.E., Madsen, H., 2010. Quantification of the spatial variability of rainfall based on a dense network of rain gauges. *Atmos. Res.* 95 (4), 441–454.
- Petersen, W.A., et al., 1999. Mesoscale and radar observations of the Fort Collins flash flood of 28 July 1997. *Bull. Amer. Meteorol. Soc.* 80, 191–216.

- Petersen, W.A., et al., 2010. Distributed disdrometer and rain gauge measurement infrastructure developed for GPM Ground Validation. American Geophysical Union, Transactions, Fall Meeting, December 2010, San Francisco, California.
- Prigent, C., 2010. Precipitation retrieval from space: a review. *C. R. Acad. Sci. Geosci.* 342, 380–389.
- Qian, T., Dai, A., Trenberth, K.S., Oleson, K.W., 2006. Simulation of global land surface conditions from 1948 to 2004. Part I: forcing data and evaluations. *J. Hydrometeorol.* 7, 953–975.
- Rabier, F., Järvinen, H., Klinker, V., Mahfouf, J.-F., Simmons, A., 2000. The ECMWF operational implementation of four-dimensional variational assimilation. I: experimental results with simplified physics. *Q. J. R. Meteorol. Soc.* 126, 1143–1170.
- Rötter, R.P., Carter, T.R., Olesen, J.E., Porter, J.R., 2011. Crop-climate models need an overhaul. *Nature Climate Change* 1.
- Ryzhkov, A., Schuur, T., Burgess, D.W., Heinselman, P.L., Giangrande, S.E., Zrníc, D.S., 2005. The joint polarization experiment: polarimetric rainfall measurements and hydrometeor classification. *Bull. Amer. Meteorol. Soc.* 86, 809–824.
- Sánchez, J.L., Gil-Robles, B., Dessens, J., Martin, E., López, L., Marcos, J.L., Berthet, C., Fernández, J.T., García-Ortega, E., 2009a. Characterization of hailstone size spectra in hailpad networks in France, Spain, and Argentina. *Atmos. Res.* 93 (1–3), 641–654.
- Sánchez, J.L., Marcos, J.L., Dessens, J., López, L., Bustos, C., García-Ortega, E., 2009b. Assessing sounding-derived parameters as storm predictors in different latitudes. *Atmos. Res.* 93 (1–3) 4th European Conference on Severe Storms – 4ECCS, 4th European Conference on Severe Storms, July 2009, pp. 446–456. doi:10.1016/j.atmosres.2008.11.006. ISSN 0169-8095.
- Sánchez, J.L., Gil-Robles, B., Dessens, J., Martin, E., López, L., Marcos, J.L., Berthet, C., Fernandez, J.T., García-Ortega, E., 2009c. Characterization of hailstone size spectra in hailpad networks in France, Spain, and Argentina. *Atmos. Res.* 93 (1–3) 4th European Conference on Severe Storms – 4ECCS, 4th European Conference on Severe Storms, July 2009, pp. 641–654. doi:10.1016/j.atmosres.2008.09.033. ISSN 0169-8095.
- Schönhuber, M., Lammer, G., Randeu, W.L., 2008. The 2D-video-vistrometer. Chapter 1 In: Michaelides, S. (Ed.), *Precipitation: Advances in Measurement, Estimation and Prediction*. Springer. ISBN: 978-3-540-77654-3.
- Scofield, R.A., Kuligowski, R.J., 2003. Status and outlook of operational satellite precipitation algorithms for extreme-precipitation events. *Mon. Weather Rev.* 18, 1037–1051.
- Sieck, L.C., Burgess, S.J., Steiner, M., 2007. Challenges in obtaining reliable measurements of point rainfall. *Wat. Res. Res.* 43, W01420.
- Sorooshian, S., Hsu, K.-L., Gao, X., Gupta, H.V., Imam, B., Braithwaite, D., 2000. Evaluation of PERSIANN system satellite-based estimates of tropical rainfall. *Bull. Am. Meteorol. Soc.* 81, 2035–2046.
- Strangeways, I., 2004. Improving precipitation measurement. *Int. J. Climatol.* 24 (11), 1443–1460.
- Strangeways, I., 2010. A history of rain gauges. *Weather* 65 (5), 133–138.
- Talagrand, O., Courtier, P., 1987. Variational assimilation of meteorological observations with the adjoint vorticity equation. Part I: theory. *Q. J. R. Meteorol. Soc.* 113, 1311–1328.
- Tapiador, F.J., 2008. A physically-based satellite rainfall estimation method using fluid dynamics modelling. *Int. J. Remote. Sens.* 29 (20), 5851–5862.
- Tapiador, F.J., 2009. Assessment of renewable energy potential through satellite data and numerical models. *Energy Environ. Sci.* 7 (2), 1142–1161.
- Tapiador, F.J., 2010. A joint estimate of the precipitation climate signal in Europe using eight regional models and five observational datasets. *J. Clim.* 23 (7), 1719–1738.
- Tapiador, F.J., Sanchez, E., 2008. Changes in the European precipitation climatologies (2070–2100) as derived by eight regional climate models. *J. Clim.* 21 (11), 2540–2557.
- Tapiador, F.J., Kidd, C., Hsu, K.-L., Marzano, F.S., 2004. Neural networks in satellite rainfall estimation. *Meteorol. Appl.* 11, 83–91.
- Tapiador, F.J., Checa, R., de Castro, M., 2010. An experiment to measure the spatial variability of rain drop size distribution using sixteen laser disdrometers. *Geophys. Res. Lett.* 37, L16803. doi:10.1029/2010GL044120.
- Tapiador, F.J., Hou, A.Y., de Castro, M., Checa, R., Cuartero, F., Barros, A.P., 2011. Precipitation estimates for hydroelectricity. *Energy Environ. Sci.* doi:10.1039/C1EE01745D.
- Thurai, M., Bringi, V.N., Petersen, W.A., 2009. Rain microstructure retrievals using 2-D video disdrometer and C-band polarimetric radar. *Adv. Geosci.* 20, 13–18.
- Thurai, M., Petersen, W.A., Tokay, A., Schultz, C., Gatlin, P., 2011. Drop size distribution comparisons between Parsivel and 2D video disdrometers. *Adv. Geosci.* 30, 3–9.
- Tokay, A., Bashor, P.G., 2010. An experimental study of small-scale variability of raindrop size distribution. *J. Appl. Meteorol. Climatol.* 49, 2348–2365.
- Tokay, A., Short, D.A., 1996. Evidence from tropical raindrop spectra of the origin of rain from stratiform versus convective clouds. *J. Appl. Meteorol.* 35, 355–371.
- Tokay, A., Kruger, A., Krajewski, W.F., 2001. Comparison of drop size distribution measurements by impact and optical disdrometers. *J. Appl. Meteorol.* 40, 2083–2097.
- Tokay, A., Wolff, D.B., Wolff, K.R., Bashor, P., 2003. Rain gauge and disdrometer measurements during the keys area microphysics project (KAMP). *J. Atmos. Oceanic Technol.* 20, 1460–1477.
- Tokay, A., Bashor, P.G., Habib, E., Kasparis, T., 2008. Raindrop size distribution measurements in tropical cyclones. *Mon. Weather Rev.* 136, 1669–1685.
- Tsuyuki, T., 1997. Variational data assimilation in the Tropics using precipitation data. Part III: assimilation of SSM/I precipitation rates. *Mon. Weather Rev.* 125, 1447–1464.
- Tuovinen, J.P., Punkka, A.-J., Rauhala, J., Hohti, H., Schultz, D.M., 2009. Climatology of severe hail in Finland: 1930–2006. *Mon. Weather Rev.* 137 (7), 2238–2249.
- Turk, F.J., Mehta, A.V., 2007. Towards improvements in short-time scale satellite-derived precipitation estimates using blended satellite techniques. In: Levizzani, V., et al. (Ed.), *Measuring Precipitation from Space: EURAINSAT and the Future*, pp. 281–290.
- Uppala, S.M., Kllberg, P.W., Simmons, A.J., Andrae, U., Bechtold, V.D.C., Fiorino, M., Gibson, J.K., Haseler, J., Hernandez, A., Kelly, G.A., Li, X., Onogi, K., Saarinen, S., Sokka, N., Allan, R.P., Andersson, E., Arpe, K., Balmaseda, M.A., Beljaars, A.C.M., Berg, L.V.D., Bidlot, J., Bormann, N., Caires, S., Chevallier, F., Dethof, A., Dragosavac, M., Fisher, M., Fuentes, M., Hagemann, S., Hólm, E., Hoskins, B.J., Isaksen, I., Janssen, P.A.E.M., Jenne, R., McNally, A.P., Mahfouf, J.-F., Morcrette, J.-J., Rayner, N.A., Saunders, R.W., Simon, P., Sterl, A., Trenberth, K.E., Untch, A., Vasiljevic, D., Viterbo, P., Woollen, J., 2005. The ERA-40 re-analysis. *Q. J. R. Meteorol. Soc.* 131 (612), 2961–3012.
- Upton, G., Brawn, D., 2008. An investigation of factors affecting the accuracy of Thies disdrometers. IOM-96, TECO 2008. World Meteorological Organization.
- van der Linden, P., Mitchell, J.F.B. (Eds.), 2009. ENSEMBLES: Climate Change and its Impacts: Summary of research and results from the ENSEMBLES project. Met Office Hadley Centre, FitzRoy Road, ExeterEX1 3 PB, UK, 160 pp.
- Veurich, E., Monesi, C., Lanza, L.G., Stagi, L., Lanzinger, E., 2009. WMO field inter-comparisons of rainfall intensity gauges. Instruments and Observing Methods, Report 99. WMO/TD-No. 1504, 96 pp.
- Vicente, G.A., Scofield, R.A., Menzel, W.P., 1998. The operational GOES infrared rainfall estimation technique. *Bull. Amer. Meteor. Soc.* 79, 1883–1898.
- Villarini, G., Mandapaka, P.V., Krajewski, W.F., Moore, R.J., 2008. Rainfall and sampling errors: a rain gauge perspective. *J. Geophys. Res.* 113, D11102. doi:10.1029/2007JD009214.
- Wilheit, T., Chang, A., Chiu, L., 1991. Retrieval of monthly rainfall indices from microwave radiometric measurements using probability distribution function. *J. Atmos. Oceanic Technol.* 8, 118–136.
- Wolff, D.B., Marks, D.A., Amitai, E., Silberstein, D.S., Fisher, B.L., Tokay, A., Wang, J., Pippitt, J.L., 2005. Ground validation for the Tropical Rainfall Measuring Mission (TRMM). *J. Atmos. Oceanic Technol.* 22, 365–380.
- Wood, S.J., Jones, D.A., Moore, R.J., 2000. Accuracy of rainfall measurement for scales of hydrological interest. *Hydrol. Earth Syst. Sci.* 4, 531–543.
- Xie, P., Arkin, P.A., 1996. Gauge-based monthly analysis of global land precipitation from 1971 to 1994. *J. Geophys. Res.* 101, 19023–19034.
- Xie, P.P., Janowiak, J.E., Arkin, P.A., Alder, R., Gruber, A., Ferraro, R., Huffmann, G.J., Curtis, S., 2003. GPCP pentad precipitation analyses: an experimental dataset based on gauge observations and satellite estimates. *J. Climate* 16, 2197–2214.
- Yuter, S.E., Kingsmill, D., Nance, L.B., Löffler-Mang, M., 2006. Observations of precipitation size and fall speed characteristics within coexisting rain and wet snow. *J. Appl. Meteorol. Climatol.* 45, 1450–1464.
- Zou, X., 1997. Tangent linear and adjoint of on-off processes and their feasibility for use in 4-dimensional variational assimilation. *Tellus* 49A, 3–31.
- Zou, X., Kuo, Y.-H., 1996. Rainfall assimilation through an optimal control of initial and boundary conditions in a limited-area mesoscale model. *Mon. Weather Rev.* 124, 2859–2882.
- Zupanski, D., 1993. The effects of discontinuities in the Betts–Miller cumulus convection scheme on four-dimensional variational data assimilation. *Tellus* 45A, 511–524.
- Zupanski, D., Mesinger, F., 1995. Four-dimensional variational assimilation of precipitation data. *Mon. Weather Rev.* 123, 1112–1127.